Hydrocarbon source rock potential in the southwestern Gulf of Suez graben

Diasty, W. Sh. El; El Beialy, S. Y. ; Mostafa, A. R.; El Adl, H. A.; Batten, David

Published in:
Marine and Petroleum Geology

DOI:
10.1016/j.marpetgeo.2016.11.012

Publication date:
2017

Citation for published version (APA):
Diasty, W. S. E., El Beialy, S. Y., Mostafa, A. R., El Adl, H. A., & Batten, D. (2017). Hydrocarbon source rock potential in the southwestern Gulf of Suez graben: Insights from organic geochemistry and palynofacies studies on well samples from the Ras El Bahar Oilfield. *Marine and Petroleum Geology*, *80*, 133-153. https://doi.org/10.1016/j.marpetgeo.2016.11.012

Accepted Manuscript

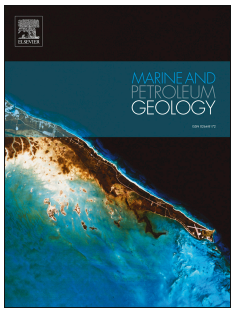

Hydrocarbon source rock potential in the southwestern Gulf of Suez graben: Insights from organic geochemistry and palynofacies studies on well samples from the Ras El Bahar Oilfield

W. Sh. El Diasty, S.Y. El Beialy, A.R. Mostafa, H.A. El Adl, D.J. Batten

PII: S0264-8172(16)30405-6

DOI: 10.1016/j.marpetgeo.2016.11.012

Reference: JMPG 2735

To appear in: *Marine and Petroleum Geology*

Received Date: 24 February 2016

Revised Date: 25 October 2016

Accepted Date: 12 November 2016

Please cite this article as: El Diasty, W.S., El Beialy, S.Y., Mostafa, A.R., El Adl, H.A., Batten, D.J., Hydrocarbon source rock potential in the southwestern Gulf of Suez graben: Insights from organic geochemistry and palynofacies studies on well samples from the Ras El Bahar Oilfield, *Marine and Petroleum Geology* (2016), doi: 10.1016/j.marpetgeo.2016.11.012.

Hydrocarbon source rock potential in the southwestern Gulf of Suez graben: Insights from organic geochemistry and palynofacies studies on well samples from the Ras El Bahar Oilfield

W.Sh. El Diasty[a*], S.Y. El Beialy[a], A.R. Mostafa[b], H.A. El Adl[a], D.J. Batten[c]

[a] Mansoura University, Faculty of Science, Geology Department, Mansoura 35516, Egypt

[b] Alexandria University, Faculty of Science, Department of Environmental Sciences, Alexandria, Egypt

[c] Department of Geography and Earth Sciences, Aberystwyth University, Penglais, Aberystwyth SY23 3DB, and School of Earth, Atmospheric and Environmental Sciences, The University of Manchester, Oxford Road, Manchester M13 9PL, UK

[*] Corresponding author, Dr. Waleed El Diasty, awaleed@mans.edu.eg, Mansoura 35516, (002) 0106 244 3492

Abstract

Palynological and biomarker characteristics of organic facies recovered from Cretaceous–Miocene well samples in the Ras El Bahar Oilfield, southwest Gulf of Suez, and their correlation with lithologies, environments of deposition and thermal maturity have provided a sound basis for determining their source potential for hydrocarbons. In addition to palynofacies analysis, TOC/Rock-Eval pyrolysis, kerogen concentrates, bitumen extraction, carbon isotopes and saturated and aromatic biomarkers enable qualitative and quantitative assessments of sedimentary organic matter to be made. The results obtained from Rock-Eval pyrolysis and molecular biomarker data indicate that most of the samples come from horizons that have fair to good hydrocarbon generation potential in the study area. The Upper Cretaceous–Paleocene-Lower Eocene samples contain mostly Type-II to Type-III organic matter with the capability of generating oil and gas. The sediments concerned accumulated in dysoxic–anoxic marine environments. By contrast, the Miocene rocks yielded mainly Type-III and Type-II/III organic matter with mainly gas-generating potential. These rocks reflect deposition in a marine environment into which there was significant terrigenous input. Three palynofacies types have been recognized. The first (A) consists of Type-III gas-prone kerogen and is typical of the Early–Middle Miocene Belayim, Kareem and upper Rudeis formations. The second (B) has mixed oil and gas features and characterizes the remainder of the Rudeis Formation. The third association (C) is dominated by amorphous organic matter, classified as borderline Type-II oil-prone kerogen, and is typical of the Matulla (Turonian–Santonian) and Wata (Turonian) formations. Rock-Eval T_{max}, PI, hopane and sterane biomarkers consistently indicate an immature to early mature stage of thermal maturity for the whole of the studied succession.

Key words: Palynofacies, Rock-Eval pyrolysis, biomarkers, Upper Cretaceous–Miocene sediments, Gulf of Suez

1. Introduction

The Ras El Bahar Oilfield is situated on the southwest bank of the Gulf of Suez, Egypt (Fig. 1). It is between the Precambrian outcrop areas of the Esh El Mallaha Range to the west and Gebel El Zeit in the northeast, 35 km south of the Ras Gharib and 50 km northwest of Hurghada (EGPC, 1996). It was discovered by the General Petroleum Company in 1962 and may be regarded as an onshore extension of the Zeit Bay Field.

There have been several studies previously on the palynology and palynofacies of Miocene deposits in the Gulf of Suez (e.g., Mahmoud, 1993; Ahmed and Pocknall, 1994; El Beialy and Ali, 2002; El Beialy et al., 2005; Soliman and Ibrahim, 2012; Soliman et al., 2012; El Atfy et al., 2013a, b, 2014). The source rock potential of Gulf of Suez formations has been reported in some detail by Rohrback (1983), Mostafa (1993), Alsharhan and Salah (1994, 1995), Barakat et al. (1997), El Diasty and Peters (2014), El Diasty et al. (2014, 2015a, 2016) and El Atfy et al. (2014), among others. Hitherto, there have not been any publications on the organic geochemistry, applied palynology or carbon isotopes of the southern sector of the Gulf of Suez. Hence this paper is a first attempt at dealing with these aspects of the Turonian–Paleocene-Lower Eocene deposits in this promising petroleum province which appears to have multiple source rock intervals that feed the Miocene and deeper reservoirs. We employ petroleum geochemistry, palynofacies analysis, total organic carbon (TOC)/Rock-Eval pyrolysis and carbon isotopes in order to determine the composition of the Turonian–Miocene source rocks in the Ras El Bahar Oilfield and the paleoenvironmental conditions they reflect.

2. Geological setting

The southern Gulf of Suez is located at the junction of the African and Arabian plates and contains several rock formations that have excellent source potential for hydrocarbons. It has a predominant southwest dip and includes several fault blocks. The structural setting is characterized by the presence of north-northwest-oriented structural trends. These trends comprise Miocene and pre-Miocene southwest-dipping fault blocks bounded by major Clysmic normal faults and dissected by cross faults (Bosworth and McClay, 2001).

The Ras El Bahar is a northwest–southeast striking horst block plunging to the north-northwest. The Clysmic trending faults, bounding the western and eastern margins of the structure,

are thrown to the southwest and northeast respectively, with an increase in the fault throw with depth from the top of the Kareem Formation to the pre-Miocene unconformity surface. The structure is dissected by east–west trending cross faults that are down thrown to the north (EGPC, 1996).

The stratigraphic units in the southern Gulf of Suez area are grouped into three main megasequences: pre-rift (Paleozoic–Eocene), syn-rift (Oligocene–Miocene), and post-rift (Pliocene–Holocene), with clear differences in their lithology, thickness, areal distribution, depositional environment, and hydrocarbon importance (Alsharhan, 2003). A generalized lithostratigraphic scheme for the study area is given in Fig. 2.

The stratigraphy of the Ras El Bahar Field was discussed by the EGPC (1996). We focus here only on the following intervals:

(1) The Upper Cretaceous Wata and Matulla formations. These overlie unconformably the Nubian succession (Fig. 2). The thickness of the Turonian Wata Formation in the Ras El Bahar (RB)-2 well is nearly 120 m. The sediments concerned are sandy and associated with shale and limestone that reflect marine transgressions. They are terminated by open marine chalky facies of the Matulla Formation, which is of Turonian–Santonian age and attains a drilled thickness of 60 m.

(2) The Paleocene-Early Eocene Esna Formation (drilled thickness 20 m). This consists of soft fossiliferous shale and thin deposits of chalky and argillaceous limestone at the top, which could be part of the Eocene Thebes Formation. It was deposited in a marine, outer sublittoral to upper bathyal setting (Schlumberger, 1984). It overlies unconformably the Sudr Chalk in the Gulf of Suez in general (Fig. 2), but in the Ras El Behar-2 well it overlies unconformably the Matulla Formation. The Thebes Formation, which in the RB-2 well is 55 m thick, consists of crystalline and cherty limestones and dolomites.

(3) The Miocene deposits. According to the National Stratigraphic Subcommittee (NSSC, 1976), the Miocene deposits in the Gulf of Suez region consist of two distinct facies: the Lower Miocene (Aquitanian) Gharandal Group and the Middle–Upper Miocene (Serravallian–Messinian) Ras Malaab Group. The Gharandal Group is subdivided from base to top into the Nukhul, Rudeis and Kareem formations (Fig. 2). No samples were available from the Nukhul Formation, so this is not considered further here.

The Rudeis Formation, originally described by the EGPC (1964), is a clastic succession above the Nukhul Formation and below the first constant anhydrite development of the Kareem Formation. It is a source of oil and also a reservoir in many oilfields in the Gulf of Suez (Schlumberger, 1984; El Ayouty, 1990). The formation, which is synonymous with the *Globigerina* marl of Said (1962), varies greatly in lithology and thickness owing to the irregular paleo-relief over which sedimentation took place. Its thickness in the type succession in the Abu Rudeis-2 well is 780

m, but in the RB-2 well it amounts to only 350 m. It overlies conformably the Nukhul Formation and underlies conformably the Rahmi/Markha Member of the Kareem Formation. It has been dated as Early Miocene (early–middle Burdigalian: e.g., Said, 1990), Early Miocene or Burdigalian (El Beialy and Ali, 2002; El Beialy et al., 2005; El Atfy et al., 2013a), and late Burdigalian–early Langhian (Soliman et al., 2012). Deposition probably took place in an open marine environment (EGPC, 1964): Evans (1988) invoked upper to upper-middle bathyal conditions based on deep water foraminifera. It consists mainly of sandy shale, fossiliferous calcareous shales with hard sandstone beds, and minor limestone intercalations. In the Rahmi-Shukeir area, it is differentiated into four formal members, Bakr, Yusr, Safra and Ayun, whereas in west central Sinai it is barely differentiated at some localities into four informal members: from oldest to youngest these are Mheiherrat, Hawara, Asl and Mreir. They all show monotonous lithologies of repeated shales, sandy shales, calcareous shales and marls, except for the Asl Member which may contain a sandy and/or limy facies that can be traced over quite long distances (NSSC, 1976).

The Kareem Formation was first described by the EGPC (1964). In its lower part it consists of the oldest stable evaporite development in the Gulf of Suez region. It is one of the main oil source rocks and contains excellent sand reservoirs in many oilfields in the Gulf (Schlumberger, 1984; El Ayouty, 1990; Alsharhan, 2003). It attains a drilled thickness of 261 m in the type section encountered in the Gharib North-2 well in the Eastern Desert (EGPC, 1964), whereas in the RB-2 well its thickness is 130 m. It overlies conformably the Ayun Musa Member of the Rudeis Formation and underlies conformably the Baba Member of the Belayim Formation. Its age is well constrained by foraminiferal and nannoplankton biostratigraphic data: these indicate Middle Miocene, Langhian–early Serravallian (15.5–14 Ma: Scott and Govean, 1985; Smale et al., 1988). Palynologically, it has been dated as Early–early Middle Miocene (El Beialy and Ali, 2002; El Beialy et al., 2005) or late Burdigalian, Langhian and Serravallian (Soliman et al., 2012). The depositional setting of the formation was shallow, partly open marine, with localized lagoonal conditions (Alsharhan and Salah, 1994), although outer shelf to upper bathyal conditions have also been inferred based on benthic foraminifera (Evans, 1988).

In the wells studied, the Kareem Formation consists mainly of highly calcareous, mostly grey mudstone grading to marl with some limestone intercalations in the upper part and massive anhydrite interbeds in the lower part. It is subdivided into an older Rahmi Member and younger Shagar Member. In the absence of the former, the undifferentiated Gharandal clastics overlying the Nukhul Formation acquire the informal name Rudeis/Kareem, whereas when the informal Asl, Hawara, Mheiherrat members of the Rudeis Formation are differentiated, the informal name Ayun Musa Member is applied to the undifferentiated Mreir and Shagar clastics (NSSC, 1976). The undifferentiated Rudeis/Kareem succession is represented in this paper by 21 cuttings samples.

The Ras Malaab Group is subdivided from base to top into the Belayim, South Gharib and Zeit formations. In this study we focus only on the Belayim Formation, samples from the other rock units being unavailable for analysis (Fig. 2).

The Belayim Formation represents the beginning of the major Miocene evaporite cycle which followed the main clastic cycle represented by the thick shales and marls of the Gharandal Group. The type section was reported from Belayim well 112-12 where it is 302 m thick. The thickness of the formation in the RB-1 well is 110 m whereas it is only 55 m in the RB-2 well. It overlies conformably the Kareem Formation and underlies conformably the South Gharib Formation. It was considered to be of Middle Miocene age by the NSSC (1976).

Deposition of the Belayim Formation may have taken place under mainly lagoonal, but partly also open marine conditions (NSSC, 1976). It consists largely of thick interbeds of white to grey, hard crystalline anhydrite, usually fossiliferous grey, green, soft to medium-hard shale, and fine to medium grained oil sand. It is subdivided into four formal members: from oldest to youngest these are Baba, Sidri, Feiran and Hamam Faraun.

3. Material and methods

Thirty-seven cuttings samples recovered from the Upper Cretaceous–Miocene succession encountered in the RB-1, -2, -4 and -5 wells were available for study. All of these were processed for palynological analysis, but owing to the small size of 17 of them it was possible to subject only 20 to TOC/Rock-Eval pyrolysis. In addition, eight bitumen extracts were analyzed using stable carbon isotope analysis and gas chromatography–mass spectrometry (GC–MS) for their content of saturated and aromatic fractions.

The Rock-Eval analysis was undertaken using a Rock-Eval 6 apparatus according to the standard technique proposed by Espitalié et al. (1977) and Behar et al. (2001) at the Egyptian Petroleum Research Institute (EPRI), Cairo, to determine TOC, hydrogen index (HI), T_{max} (°C) and other calculated ratios indicative of kerogen type and petroleum generative potential (Hunt, 1996).

Palynological processing of the 37 cuttings samples involved modified standard techniques (cf. Traverse, 2007): 10–15 g of each sample were disaggregated by crushing in a porcelain mortar to increase the surface area of reaction with HCl (conc. 35 %) and HF (conc. 45 %) to remove carbonates and silicates. The organic matter (kerogen) recovered was separated from any remaining inorganic material by sieving through a 125 μm brass sieve, the residue being collected on a 10 μm nylon sieve. No oxidation or staining was applied to any of the residues. A few drops of polyvinyl alcohol were added to each residue in order to disperse the organic components, which were allowed to dry on a cover slip. This was then inverted onto a microscope slide on which a few drops

of Elvacite 2044 acrylic resin dissolved in xylene had been placed. Elvacite is a useful mounting medium in the context of our work because it does not fluoresce in ultraviolet light. A drop of liquefied phenol was added to all sieved and un-sieved residues to inhibit microbial growth. Selected palynomorphs and types of palynodebris were photographed using an Olympus Microscope (BX10): these are illustrated below under transmitted light at different magnifications. 200 kerogen particles were counted in order to obtain qualitative and semi-quantitative data on the dispersed organic matter. Palynomorphs were excluded from these counts because they were so rarely encountered.

Using dichloromethane as a solvent for 72 h, organic extracts from pulverized rock samples were fractionated by column chromatography into saturated, aromatic, and nitrogen, sulphur and oxygen components (NSO) in a silica gel alumina column after the precipitation of asphaltenes using a 40× excess of hexane. Bulk stable carbon isotope analysis for the five Miocene extracts of saturated and aromatic fractions was determined using the combustion technique of Sofer (1980) and carried out on a Finnigan Delta Plus XL instrument. Results are reported against the PDB standard.

The GC-MS of saturated and aromatic hydrocarbon fractions was undertaken on a Hewlett Packard 6890 Series coupled to a Hewlett Packard 5973 Series Mass Selective Detector (equipped with a 30 m × 0.25 mm i.d. HP-5MS column with a film thickness of 0.25 µm and using helium as a carrier gas). The oven was held for 1 min at 35°C, then increased from 35 to 120°C at 10°C/min and from 120 to 300°C at 3°C/min, with a final holding time of 30 min at 300°C. The Selective Ion Monitoring (SIM) mode permitted specific ions to be monitored, such as hopanes (*m/z* 191) and steranes (*m/z* 217). Biomarker ratios were calculated from peak areas of appropriate mass fragmentograms in the saturated and aromatic hydrocarbon fractions (Peters et al., 2005). All of these bulk and organic geochemical analyses were undertaken by GeoMark Research Ltd, Houston, Texas (USA).

4. Results and discussion

4.1. Source rock bulk geochemical characteristics

TOC values of the samples analyzed range between 1.06 and 3.80% (Table 1), indicating good to very good source rocks. It is apparent that all of the samples have high quality TOC (wt%) and contain more than the minimum amount for a viable source rock (Fig. 3). The Turonian samples at depths 2652 m and 2703 m contain the highest measured TOC (3.80% and 3.34%) as shown in Table 1. The high TOC values for these two samples can be linked to the depositional environment and redox conditions (see below).

S_1 values represent poor to fair generating potential as they range from 0.01 to 0.72 mg HC/g rock, except for the two Turonian samples where S_1 records the highest values (1.85 and 1.68), which indicates a good source rock (Table 1) and perhaps also oil that has migrated into this formation in well RB-2. All of the samples analyzed have low S_1 relative to high TOC values, indicating that they contain indigenous hydrocarbons, but the presence of migrated hydrocarbons cannot be ruled out (Hunt, 1996).

The hydrogen index (HI) readings range from 75 to 389 mg HC/g TOC, indicating a mixed Type-III and II/III kerogen for the Miocene and Paleocene-Lower Eocene samples and Type II/III to borderline Type II kerogen for the two Turonian samples (Table 1). The observed variations in organic matter input (from marine to terrigenous or mixed characters) and decrease in HI values may result from changes in water depth and associated variations in the redox conditions during the deposition of these strata (Demaison et al., 1983).

Kerogen plots can be anywhere on the van Krevelen diagram and need not fall on any of the indicated maturation curves owing to the combined effects of diagenesis, thermal maturity and differing input of organic matter (Peters and Cassa, 1994). The HI was plotted versus the oxygen index (OI) on a modified van Krevelen diagram (Fig. 4) to determine the origin of the organic matter. The kerogen types appear to be of mixed Type-II/III (oil- and gas-prone) to Type-III (gas-prone).

4.2. Palynofacies analysis

Our palynofacies analysis is focused mainly on the Upper Cretaceous Wata and Matulla formations for which no data have been available previously from the southern Gulf of Suez. However, a detailed palynofacies analysis was undertaken by El Diasty et al. (2014) on the same interval in the central Gulf of Suez. The palynological content of the Paleocene-Early Eocene Esna Formation in the gulf has also been studied for the first time, albeit based on only one sample. As noted above, the Miocene strata of the Rudeis and Kareem formations have been investigated palynologically previously. Here we include observations on the palynology of the overlying Miocene Belayim Formation for which hitherto there have been no palynological reports despite its importance from a petroleum viewpoint.

Significant variations in palynofacies character can only be assessed by counting and analyzing numerical data (Tyson, 1993). Palynomorph counts are plotted on Table 2. Unfortunately palynomorphs were scarce in nearly all of the samples, hence diminishing their value for assessing past vegetation and paleoclimatic changes (e.g., El Beialy et al., 2005).

The palynofacies data recorded from all 37 cuttings samples examined are summarized in Table 3 and illustrated diagrammatically in Figs. 5–7. Overall the organic matter is relatively well-preserved. Finely disseminated pyrite is present in a few of the preparations. Examples of some of the components are illustrated in Figs. 8–10.

The ternary diagram AOM-phytoclast-palynomorph (APP) (Fig. 5) of Tyson (1993, 1995) shows a clear separation of various groups of assemblages. The clusters refer to three main palynofacies associations (see details in the following paragraphs). Association-A samples lie mainly within field II, which indicates a marginal dysoxic–anoxic basin, and hence is classified as Type-III, gas-prone kerogen (Tyson, 1995). Those of Association-B fall within palynofacies fields VI and II with a clear transition from a proximal suboxic–anoxic shelf yielding Type-II kerogen to a gas-prone marginal dysoxic–anoxic basin. Association-C samples lie mainly in the field IX, indicating a distal suboxic–anoxic basin and Type-II, highly oil-prone kerogen. These three associations were differentiated on the basis of relative abundances of the particulate organic matter recovered.

4.2.1. Palynofacies association-A

This association was recovered from 21 samples: 16 from the Rudeis-Kareem succession and five from the overlying Belayim Formation. It is dominated by terrigenous amorphous organic matter (AOMT; Batten, 1996a) and phytoclasts (mainly cuticles and tracheids). The AOMT percentage usually exceeds 60%, except in sample RB2.2, 1932–1935 m, in which it amounts to only 44% (Table 3; Fig. 6).

Morphologically, the majority of the AOM particles have a granular appearance with angular to sub-angular outlines, while others have no distinct margins. They are fairly well to well preserved and vary from light brown (Fig. 8A) to dark brown masses having a clotted aspect. The phytoclasts consist mainly of pale brown to brown, fairly well-preserved fragments that include cuticles (Fig. 8B) as well as other tissues (Fig. 8C, D). Elongate lath-shaped and tabular tracheids are also present. The content of land-plant debris recovered from the Kareem Formation varies: it is most abundant in the upper part. Rare occurrences of equidimensional opaque particles were also encountered.

In addition to AOMT and phytoclasts, this association contains rare pollen grains, fungal spores, trilete spores, dinocysts and microforaminiferal test linings, overall averaging between 2 and 3% of the assemblage. They are more common (up to 7%) in some samples from the RB-4 well. No marked change in the palynofacies content between the Rudeis and Kareem formations was detected: most of the dinocyst taxa recorded from the former were also encountered in the Kareem Formation. Some of these were identified as *Sumatradinium* sp. cf. *S. hispidum* (Fig. 8E),

Cordosphaeridium minimum (Fig. 8F) and *Melitasphaeridium choanophorum* (Fig. 8J). Gonyaulacoid dinocysts (e.g., *Spiniferites* sp. cf. *S. pseudofurcatus* and *S.* sp. cf. *S. ramosus*, Fig. 8G–I) are more abundant than peridinioid dinocysts (e.g., *Selenopemphix brevispinosa* and *S. nephroides*).

4.2.2. Palynofacies association-B

This association was recovered from 10 samples representing the lower part of the Rudeis Formation. It contains a mixture of marine amorphous organic matter (AOMA; Batten, 1996a) and AOMT, but platy, structureless AOM of aquatic derivation dominates (>50%) except in samples 11 and 13 from the RB-2 well (Table 3; Fig. 6). Under a transmitted light microscope the amorphous marine organic matter can be differentiated from structureless, degraded phytoclasts in having a thicker, darker appearance. In addition, degraded phytoclasts often show remnants of their original morphology, such as cell walls (El Beialy et al., 2016). The morphology of the AOM ranges between sub-angular particles with neat boundaries to diffuse, fluffy particles (Fig. 9A, B). Most consists of clotted and/or lumpy textures suggesting that it has both marine and non-marine origins (El Atfy et al., 2014). Phytoclasts and palynomorphs (both miospores and dinoflagellates: Fig 9A and B respectively) are scarce. Other characteristic palynomorphs for this association are illustrated in Fig. 9C–E.

AOM comprises more than 50% of the palynofacies from the lower part of the Rudeis Formation, which is consistent with previous work on this part of the formation elsewhere (El Atfy et al., 2014). Deposition is considered to have taken place under open marine conditions, as reported by the EGPC (1996).

4.2.3. Palynofacies association-C

This association was recorded from six samples representing the Wata, Matulla, and Esna formations. AOM is the most common kerogen type (Table 3; Fig. 6). Dominance of AOM (usually more than 90%) indicates suboxic to anoxic conditions during sedimentation (e.g., Tyson, 1995; Batten, 1996a). This ranges from yellow to light brown in transmitted light (Fig. 10A, B). All AOM in this association is much more uniform in appearance by comparison with that encountered in associations A and B; margins are indistinct and there is no structure to any of it. Characteristic palynomorphs include those illustrated in Fig. 10C–E.

4.3. Paleoenvironmental interpretation

Organic particles in sediments and hence alterations in the composition of palynofacies may be used to document environmental changes under different climatic and sedimentary settings, especially when linked to existing sedimentological interpretations (e.g., Batten, 1996a; Carvalho et al., 2006, 2013). Many spores and pollen grains recorded from Late Cretaceous and younger deposits are morphologically similar to those of modern taxa and can, therefore, considerably enhance paleoenvironmental interpretations, but their very limited recovery from deposits of this age-range in the Gulf of Suez area means that any conclusions drawn are inevitably tentative (El Beialy et al., 2005; El Atfy et al., 2013b). Their scarcity in the palynofacies recorded herein means that there is little on which even to base any discussion of this sort: the dinocysts are more informative (see below). Their rare occurrence may be attributable to the low elevation of the nearest land surface coinciding with a rapid sea level rise and restricted transport of terrigenous debris at the time of deposition (Pearson et al., 1982). Hence, our paleoenvironmental deductions are based mainly on the composition of the palynofacies and the sediments with which they are associated, with the proviso that these must be regarded as tentative because our study involves only cuttings samples.

Taking into account previous observations on the environments represented by the rocks investigated, it is apparent that the thin units of the Turonian Wata Formation reflect deposition in the marine realm. This formation is succeeded by the Turonian–Santonian Matulla Formation, which was deposited under open marine conditions, and is overlain conformably by the Campanian–Maastrichtian Brown Limestone and Sudr formations (Fig. 2), which accumulated in deeper marine conditions. Deposition was then terminated at the end of the Cretaceous Period, the next unit being the Paleocene-Early Eocene Esna Formation, which rests unconformably on the Sudr Formation.

As already discussed, the Late Cretaceous and early Paleogene palynofacies contain an abundance of AOM, reflecting deposition in a distal suboxic–anoxic basin. The pre-rift succession is terminated by the deposition of the Eocene shelf carbonates of the Thebes Formation. By the end of the Late Eocene (Fig. 2), the Tethys Sea was restricted to the north of the Gulf of Suez area and rifting of the gulf took place, resulting in the erosion of strata, which continued during the separation of the African Plate and Sinai Sub-plate in the latest Oligocene–Early Miocene (Boukhary et al., 2012).

The Tethys Sea then transgressed over the eroded blocks depositing basal Miocene clastics and Rudeis carbonate shelf facies on high areas, while deeper marine muds and sands accumulated in the low areas around the highs. The great thickness and lithological variations encountered in the

Rudeis Formation is a reflection of the irregular paleo-relief over which sedimentation took place (Alsharhan and Salah, 1994). These are also reflected in its organic content and the differing environments in which it accumulated. They record the earliest phase of sedimentation in a syn-rift basin as revealed in the APP ternary plot in which Association-B samples are located in palynofacies fields VI and II (Fig. 5). As previously noted, these represent a transition from a proximal suboxic–anoxic shelf to a marginal dysoxic–anoxic basin.

The next depositional event in the study area is the accumulation of the Kareem Formation in an open marine, partly lagoonal environment, beginning with the older Markha/Rahmi Member (NSSC, 1976), which consists of a thin anhydrite bed intercalated with shales and marls, and the overlying Shagar Member, which is represented by fossiliferous shales and marls with occasional thin limestone intercalations, and locally minor sands. The syn-rift sedimentary succession is terminated by the deposition of the Belayim Formation, which accumulated in a lagoonal to shallow marine setting (Alsharhan and Salah, 1994; EGPC, 1996).

The Rudeis-Kareem and Belayim samples characterize palynofacies association-A as discussed earlier. This reflects deposition in a marginal dysoxic–anoxic environment, suggesting close proximity to a fluvio-deltaic source of land-plant debris as implied by the APP ternary plot, field II (Fig. 5), despite the scarcity of miospores. The similarity in the palynofacies content of both the upper Rudeis and Kareem formations is likely to reflect similar depositional conditions. The difference that is apparent between the palynofacies associated with the lower and upper Rudeis Formation coincides with the mid-Rudeis tectonic event (Hughes et al., 1992). This was a major reactivation of the rift that involved the segmentation and rotation of pre-existing fault blocks into smaller units (Beleity, 1982).

The Rudeis Formation, particularly the upper part, is considered to have been deposited in relatively deep water based on the presence of some of the dinocysts encountered, the *Achomosphaera/Spiniferites* complex, *Operculodinium*, and *Cleistosphaeridium* suggesting outer neritic environments. The sporadic occurrence of the heterotrophic taxa *Selenopemphix* and *Lejeunecysta* suggests nutrient-rich surface waters (El Atfy et al., 2014). Species of the open marine dinocyst *Spiniferites* are most common when angiosperm pollen grains of the *Poaceae* are also present.

4.4 Palynofacies and geochemical correlation

Integration of palynological and geochemical data enables the potential of a given horizon as source of hydrocarbons to be determined more reliably than either of these on their own (Batten, 1996b). AOM is the single most important source of hydrocarbons and the main type of kerogen in

source rocks (e.g., Thompson and Dembicki, 1986; Mendonça Filho et al., 2012). Differences in the chemistry of the original organic source of AOM result in differences in its petroleum potential (Batten, 1996b). The van Krevelen diagram (Fig. 4) shows how the loss of hydrogen makes oil-prone Types-I and II kerogen change to gas-prone Type-III kerogen (Hunt, 1996).

Geochemical analyses were carried out on 20 samples from the depth interval 1407–2706 m through the Wata, Esna, Rudeis, Kareem and Belayim formations in the RB-1, -2, -4 and -5 wells. Raw data plotted on the van Krevelen diagram show that the Miocene samples are of mixed Type-III to Type-II/III kerogen and hence have potential for gas generation whereas the two Turonian samples contain Type II/III to borderline Type-II oil-prone kerogen.

Palynofacies association-A samples indicate Type-III gas-prone kerogen, low HI values (88–261 mg HC/g TOC) except for sample RB2.2 (Table 1), and low AOM values (Table 3). Samples yielding Palynofacies association-C have the greatest values of HI and AOM, indicating oil-prone Type-II to Type II/III kerogens based on the Rock-Eval HI values (Peters ad Cassa, 1994). As shown in Fig. 7, the data obtained from the palynofacies analysis correlate well with those from Rock-Eval pyrolysis except for the Paleocene-Early Eocene Esna Shale, which is regarded as Type-III gas-prone based on organic geochemistry but contains Type-II kerogen based on palynofacies data. However, the latter derive from only one sample and are not necessarily typical of the formation as a whole, which is not regarded as an oil source rock according to Rock-Eval data.

TOC values are high, ranging between 2.65 and 3.80% in the three studied samples RB2.5, RB2.18 and RB2.20, and HI readings range from 323 to 389 mg HC/g TOC, indicating Type-II oil-prone kerogen, as interpreted from Peters and Cassa (1994). High AOM content is also recorded (Table 3; Fig. 7). The increasing content of TOC, HI and AOM in these samples suggests enhanced preservation associated with more reducing conditions.

Data from the Matulla Formation are unavailable (see Table 1) owing to the poor recovery of samples from the drilled wells.

4.5. Stable carbon isotope composition ($\delta^{13}C$ %)

Many types of marine and terrigenous organic matter can be distinguished using the stable carbon isotope ratios of the C_{15+} saturated and aromatic hydrocarbons. This distinction refers to the provenance of the organic matter and not to its depositional environment (Peters et al., 2005). In this study, a stable carbon isotope analysis was carried out only on the Miocene extracts (Table 4) because there have been no previous studies to determine whether potential source rocks of this age might be indicated. The carbon isotope values of the saturated fractions range from -28.26 to -26.67‰ and the aromatic fractions from -27.81 to -25.32‰ (Table 4). The carbon isotope data

show that the two samples from the Kareem Formation, RB4.4 and RB5.1, differ markedly (Table 4). This may reflect significant differences in organic matter input and/or depositional environment. The RB5.1 bitumen sample is much heavier isotopically than the other Miocene samples (Table 4), indicating particularly anoxic marine conditions (see section 4.6).

The isotopic relationship for terrigenous oils differs from that of marine oils and can be formalized by a statistical parameter called the canonical variable (CV; Sofer, 1984) cited as: CV = $-2.53\delta^{13}C_{sat} + 2.22\delta^{13}C_{aro} - 11.65$. The overall negative CV values (-2.20 to -0.39) of the Miocene samples (Table 4) indicate a transitional marine depositional environment. This is based on the fact that the CV value above 0.47 indicates organic matter with a terrigenous source, while values below 0.47 signify marine organic matter (Sofer, 1984).

The combined results of the palynofacies and isotopic analyses can be used to infer depositional environment. The bulk stable carbon isotope data for the Miocene extracts is consistent with the palynofacies results where the samples belong to palynofacies associations-A and -B: these represent a transition from a proximal suboxic–anoxic shelf to a marginal dysoxic–anoxic basin.

4.6. Biomarker characteristics

4.6.1. Depositional environments

Fig. 11 shows the *m/z* 191 and *m/z* 217 mass fragmentograms of saturated hydrocarbon fractions for three selected extract samples from the RB-2 well. High tricyclic terpanes in the *m/z* 191 chromatograms are usually common in marine environments and believed to have originated from algae and bacteria (Zumberge, 1987; Burwood et al., 1992; Hanson et al., 2000; El Diasty and Moldowan, 2012). Low values of C_{19}/C_{23} (0.04–0.06) and high values of C_{25}/C_{26} (1.20–1.49), C_{22}/C_{21} (0.56–0.68) and C_{24}/C_{23} (0.46–0.48) have been reported for the Cretaceous extracts and indicate a marine environment (Peters et al., 2005; Volk et al., 2005) and more carbonate-rich rocks. By contrast, the Miocene samples have different ratios for the same parameters (Fig. 12). Fig. 12 shows that the Cretaceous and Paleocene-Lower Eocene carbonate-rich rock extracts have abundant C_{22}/C_{21} tricyclic terpanes compared with those from the Miocene Rudeis and Kareem extracts. The fairly high values for C_{19}/C_{23} (0.05–0.16) and C_{25}/C_{26} (0.94–1.20) and C_{24}/C_{23} (0.52–0.61) suggest mixed organic matter in a marine environment.

Relatively abundant C_{24} tetracyclic terpane has been regarded as common in carbonate and evaporite depositional environments (Palacas et al., 1984; Connan and Dessort, 1987). However, this compound is believed to indicate terrigenous organic matter and support the influx of higher plant material in a source rock (Philp and Gilbert, 1986; Mello et al., 1988). The C_{24} tetracyclic/C_{26} tricyclic values can easily be used to differentiate the Miocene from the Cretaceous–Paleocene-Lower Eocene samples (Table 4). All the Miocene samples have C_{24}/C_{26} ratios of ≥1.0, whereas

those from the Cretaceous–Paleocene-Lower Eocene succession are mostly lower than 1.0. These low values for the latter group could be a marker for marine organic matter (Mello et al., 1988; Philp and Gilbert, 1986). However, owing to poor chromatographic separation of the Wata sample (Fig. 11) the C_{24} tetracyclic coelutes with the first eluting C_{26} tricyclic make quantification difficult and introduce a potential error in the ratio.

The terpane (*m/z* 191) mass chromatograms for the samples analyzed show dominant pentacyclic terpanes with high intensities of C_{30} hopane and decreasing relative proportions of extended hopanes from C_{31} to C_{35} (Fig. 11).

The oleanane/hopane ratio is a common source and age indicator because oleanane is derived from flowering plants of Late Cretaceous or, more commonly, Tertiary age (Ekweozor and Telnaes, 1990; Moldowan et al., 1994). It is evident that oleanane is absent from the Cretaceous and Paleocene-Lower Eocene samples studied here. This may be a result of the dominance of marine depositional conditions with negligible terrigenous influx. By contrast, the Miocene extracts have insignificant amounts of oleananes (0.05–0.13: Table 4), confirming significant terrigenous input to their source rocks (Fig. 11). Consistent with this, the Ts/Tm ratios for the Cretaceous and Paleocene-Lower Eocene extract samples range from 0.35 to 0.36 (<0.5: Table 4), indicating a clay-poor, marine-carbonate depositional environment (Mello et al., 1988). The ratios for the Miocene samples are greater than 0.5 (up to 0.73), indicating marine deposits that received an input of terrigenous organic matter.

The high homohopane index ($C_{35}S/C_{34}S>1.3$) for the Cretaceous–Paleocene-Lower Eocene extracts is interpreted to indicate highly reducing marine conditions during deposition (Peters and Moldowan, 1991; Sinninghe Damsté et al., 1995) and derivation from bacteriohopanetetrol as well as from other hopanoids in bacteria (Ourisson et al., 1984). As shown in Table 4, $C_{35}S/C_{34}S$ homohopane ratios of Cretaceous–Paleocene-Lower Eocene extracts are higher than those for the Miocene extracts and all samples are more than 1.0, except for one from the RB5.1 well, which has a very high C_{35}/C_{34} hopane ratio of 2.67, indicating that these rocks might reflect a reducing environment. This interpretation is consistent with the norhopane/hopane, sterane/hopane and C_{31}/hopane ratios (Table 4). In addition to the very high C_{35}/C_{34} hopane ratio for the Kareem RB5.1 extract, a high salinity is also indicated [very high gammacerane ratio of 0.60 (Table 4), the highest in this study], resulting in a low eubacterial population, as manifested by a very high sterane/hopane ratio (3.04, Table 4), which is consistent with algal (high C_{27} regular sterane) marine matter and a reducing environment.

The low gammacerane indices reported for the Miocene material (<0.20: Table 4), indicate deposition under normal salinity for the corresponding source rocks (Sinninghe Damsté et al., 1995). By contrast, the abundance of gammacerane recorded from the Cretaceous–Paleocene-Lower

Eocene samples (>0.20: Table 4) suggests a stratified water column in marine carbonate–evaporite conditions of deposition (Mello et al., 1988; ten Haven et al., 1989). The abundance of marine organic matter during the deposition of the Cretaceous and Paleocene-Lower Eocene sediments is also confirmed by the presence of C_{30} 4-desmethyl steranes (Fig. 11: Moldowan et al., 1985).

The ratios of dibenzothiophene/phenanthrene (DBT/P) in the aromatic hydrocarbon fraction exhibit wide variations in the samples studied. The Miocene extracts have DBT/P ratios of < 0.5, which is lower than those recorded for the Cretaceous–Paleocene-Lower Eocene samples (Table 4), indicating marine siliciclastic source rocks (Hughes et al., 1995).

The relative concentrations and distribution patterns of regular steranes are used as source parameters that can also differentiate depositional settings (Peters et al., 2005). The distribution patterns with similar contents of regular steranes C_{27}, C_{28} and C_{29} in the Cretaceous–Miocene extracts (Table 4) suggest a greater contribution of algal organic input and terrigenous plant matter to the organic source (El Diasty and Moldowan, 2012).

Rohrback (1983) regarded the Upper Cretaceous Brown Limestone as the major oil source rock and the Eocene Thebes units as probable source rocks. This is consistent with Mostafa (1993), El Diasty and Peters (2014) and El Diasty et al. (2015) who considered that the oils in the central Gulf of Suez, including the Belayim oils, closely correlated with source rocks from the Brown Limestone and Thebes Formation.

There are other potential oil-producing source rocks in the Gulf of Suez. The geothermal gradient increases from north to south, and Rohrback (1983) found the most mature oils in the south. Some of these other sources may come into play increasingly in that direction. However, whereas rocks of sufficient maturity may generate oil, they do not necessarily have the physical properties to expel it. Instead it may be swept up by migrating oils, altering some of their geochemical characteristics in the process. El Diasty and Peters (2014) showed that ZEC3 oil from the southern Gulf of Suez has both marine and terrestrial characteristics (Family II oil). They also considered the Lower Miocene Rudeis Formation to be the best candidate for generating oils of this family in the southern part of the gulf.

Despite the poor chromatography, the mass fragmentograms of *m/z* 191 and *m/z* 217 of the Wata bitumen extract (Fig. 11) are very similar to the triterpanes and steranes of Belayim marine oils from wells BM-70 and BM-49 (El Diasty et al., 2015a) and to all of the oils discussed by Rohrback (1983), particularly the most immature oil from Ras Bakr (Nubian reservoir), which is situated in the northern part of the southern sector of the Gulf of Suez. The bitumen in the Wata extracts may be from migrating oil, which the GC-MS of the Wata sample (Fig. 11) strongly supports. This non-indigenous oil in the rocks analyzed will undoubtedly contain contaminating biomarkers that may adversely affect assessments of hydrocarbon source potential. It is worth

noting here that the characteristics of the Upper Cretaceous source rocks are very similar to the Family-I oils of El Diasty and Peters (2014) and those of the Cleopatra bitumen and other younger mummies.

In this paper, the extracts from the Rudeis cuttings have biomarker signatures that differ from the Family II oils of El Diasty and Peters (2014). This difference could be the result of the genetic composition of the source rock lithofacies, organic facies and thermal maturity, all of which can cause variations in oil characteristics in the same oil family. By contrast, the other Miocene source rock extracts are genetically related to the biomarker signature of Family-II oils (El Diasty and Peters, 2014) and the Pasenhor mummy, emphasizing that bitumen from Gebel El Zeit was used by Egyptians at least as early as the ninth century BC for mummification (El Diasty et al., 2015b).

4.6.2. Thermal maturity

Rock-Eval data indicate that the majority of samples lie within the marginally mature stage. The production index (PI = $S_1/[S_1+S_2]$) is less than 0.1 at the top of the oil window and reaches approximately 0.4 at the bottom (Peters and Cassa, 1994). The PI is in the range of 0.01 to 0.28 with the majority of samples being less than 0.10, and the T_{max} values vary within the range of 416–438°C, which suggest an immature to early mature source rock. The maturity estimates suggested by the T_{max} and PI values are slightly inconsistent, probably owing to a small amount of associated petroleum generation but also perhaps to the expulsion of some of the generated petroleum from the rocks, both of which could have affected the Rock-Eval pyrolysis results (Fig. 13).

Biomarker parameters supplement our understanding of the thermal maturity of the source rocks. C_{31}- or C_{32}-homohopanes are key maturity indicators. In this study, the ratio of 22S/(22S+22R) for C_{32} 17α(H),21β(H)-homohopanes ranges from 0.50 to 0.59 (Table 4; 0.57–0.62 = equilibrium), indicating that all the extracts have a thermal maturity within the early oil window (Mackenzie and Maxwell, 1981; Peters et al., 2005).

The isosterane content is primarily related to maturity, which transforms the biologic ααα forms (normal steranes) into αββ forms (Seifert and Moldowan, 1986; Rullkötter and Marzi, 1988). The values of 20S/(20S+20R) and αββ/(αββ+ααα) of the C_{29} steranes average 0.38 and 0.41 in the RB-2 well. Therefore, based on the Rock-Eval PI and T_{max}, 22S/(22S+22R) hopanoids, 20S/(20S+20R) and αββ/(αββ+ααα) of the C_{29} steranes ratio data, all of the samples exhibit an early mature thermal stage (Fig. 14).

The Cretaceous–Miocene source rock maturity was also estimated using aromatic maturity parameters. The methylphenanthrene index is calculated using the peak areas of methylphenanthrene (MP) and phenanthrene (P) from *m/z* 192 and *m/z* 178 fragmentograms, respectively (Cassani et al., 1988). The values of the MPI-1 range from 0.58 to 0.96 and the

calculated vitrinite reflectance %Rc ranges from 0.75 to 0.97 (Table 4), also indicating that these rocks from the Ras El Bahar Oilfield are at the early oil window.

5. Summary and conclusions

A detailed optical microscopic, organic geochemical and carbon isotope analysis of 37 cuttings samples from the Upper Cretaceous and Tertiary deposits encountered in the Ras El Bahar Oil Field, southern Gulf of Suez, Egypt, has enabled the evaluation of organic matter provenance and source rock potential of the Wata, Matulla, Esna and Belayim formations for the first time. We draw the following conclusions from our study:

1. The Upper Cretaceous, Paleocene-Lower Eocene and Miocene succession includes deposits containing high quality TOC (wt%), indicating the presence of good source rocks that could generate significant quantities of hydrocarbons in the study area.
2. Rock-Eval pyrolysis results suggest an early mature Type II/III to borderline Type II kerogen for the Cretaceous samples, Type-III for the Paleocene-Lower Eocene Esna sample, and mixed Type-III kerogen (gas-prone) to Type-II/III (oil-gas-prone) for the Miocene deposits. However, it must be noted that migrating oil into the rocks analyzed may have affected indications of their potential as commercial source rocks.
3. Palynomorphs are scarce throughout the succession. The palynofacies of the Miocene rock units investigated contain minor marine components in the form of dinoflagellate cysts and rare microforaminiferal test linings. The persistent occurrence of AOM indicates that dysoxic to anoxic conditions prevailed throughout deposition of the sediments examined.
4. Three main palynofacies associations were identified. The first (A), dominated by AOMT and phytoclasts and classified as Type-III gas-prone kerogen, was encountered through the Miocene Belayim, Kareem and upper Rudeis formations. The second (B) was recorded down through the remainder of the Rudeis Formation and considered to comprise mixed Type-II/III kerogen. Association C, which consists of more than 90% marine AOM and hence is classified as Type-II, highly oil prone kerogen, encompasses the Esna (Paleocene-Early Eocene), Matulla (Turonian–Santonian) and Wata (Turonian) formations.
5. Biomarker analyses suggest that the Late Cretaceous–Early Paleogene source rocks reflect deposition in a highly reducing, stratified water column in marine carbonate–evaporite environments. The Miocene extracts indicate mixed marine–terrigenous environments based on stable carbon isotope composition and biomarker analyses.
6. The combination of detailed microscopic and geochemical analyses serves to emphasize their importance in evaluating organic matter richness, kerogen type, and thermal maturation levels of

the samples from the Ras El Bahar Oilfield. Both showed close agreement and hence provide a sound basis for drawing paleoenvironmental and source potential conclusions.

Acknowledgements

The Egyptian General Petroleum Company kindly supplied the samples and essential data used in this study. We are indebted to StratoChem (New Maadi, Cairo) and GeoMark (Houston, Texas) laboratories for their continuing analytical support. Geoffrey Abbott (Associate Editor), Jennifer Galloway, Jim McEvoy and an anonymous reviewer are gratefully acknowledged for their constructive comments, which substantially improved the quality of this manuscript.

References

Ahmed, A.B.A., Pocknall, D.T., 1994. The application of palynology to exploration in the Miocene–Pliocene sequence in the Gulf of Suez, Egypt. Proceedings of 12th Petroleum Exploration and Production Conference. Egyptian General Petroleum Corporation, EGPC, Cairo, pp. 468–481.

Alsharhan, A.S., 2003. Petroleum geology and potential hydrocarbon plays in the Gulf of Suez rift basin, Egypt. American Association of Petroleum Geologists, Bulletin 87, 143–180.

Alsharhan, A.S., Salah, M. G., 1994. Geology and hydrocarbon habitat in rift setting, southern Gulf of Suez, Egypt. Bulletin of Canadian Petroleum Geology 42, 312–331.

Alsharhan, A.S., Salah, M.G., 1995. Geology and hydrocarbon habitat in rift setting: northern and central Gulf of Suez, Egypt. Bulletin of Canadian Petroleum Geology 43, 156–176.

Barakat, A.O., Mostafa, A., El-Gayar, M.S., Rullkötter, J., 1997. Source-dependent biomarker properties of five crude oils from the Gulf of Suez, Egypt. Organic Geochemistry 26, 441–450.

Batten, D.J., 1996a. Palynofacies and palaeoenvironmental interpretation. In: Jansonius, J., McGregor, D.C. (Eds.), Palynology: Principles and Applications. American Association of Stratigraphic Palynologists' Foundation, Dallas, 1011–1064.

Batten, D.J., 1996b. Palynofacies and petroleum potential. In: Jansonius, J., McGregor, D.C. (Eds.), Palynology: Principles and Applications. American Association of Stratigraphic Palynologists' Foundation, Dallas, 1065–1084.

Behar, F., Beaumont, V., De, B., Penteado, H.L., 2001. Rock-Eval 6 technology: performances and developments. Oil & Gas Science and Technology: Revue de l'Institut Français du Pétrole 56 (2), 111–134.

Beleity, A., 1982. The composite standard and definition of paleo events in the Gulf of Suez. Proceedings of 6th Petroleum Exploration and Production Conference. The Egyptian General Petroleum Corporation, EGPC, Cairo, pp. 181–198.

Boukhary, M., Abd El Naby, A., Faris, M., Morsi, A., 2012. Plankton stratigraphy of the Early and Middle Miocene Kareem and Rudeis formations in the central part of the Gulf of Suez, Egypt. Historical Biology 24, 49–62.

Bosworth, W., McClay, K.R., 2001. Structural and stratigraphic evolution of the Gulf of Suez Rift, Egypt: a synthesis. In: Ziegler, P.A., Cavazza, W., Robertson, A.H.F., Crasquin-Soleau, S. (Eds.), Peri-Tethys Memoir 6: Peri-Tethyan Rift/Wrench Basins and Passive Margins. Memoires du Museum National d'Histoire Naturelle, Paris 186, 567–606.

Burwood, R., Leplat, P., Mycke, B., Paulet, J., 1992. Rifted margin source rock deposition: a carbon isotope and biomarker study of a West African Lower Cretaceous "lacustrine" section. Advances in Organic Geochemistry 1991. Organic Geochemistry 19, 41–52.

Cassani, F., Gallango, O., Talukdar, S., Vallejos, C., Ehrmann, U., 1988. Methylphenanthrene maturity index of marine source rock extracts and crude oils from the Maracaibo Basin. Organic Geochemistry 13, 73–80.

Carvalho, M.A., Cabral Ramos, R.R., Crud, M.B., Witovisk, L., Kellner, W.A., Silva, H.P., Grillo, O.N., Riff, D., Romano, S.R., 2013. Palynofacies as indicators of paleoenvironmental changes in a Cretaceous succession from the Larsen Basin, James Ross Island, Antarctica. Sedimentary Geology 295, 53–66.

Carvalho, M.A., Mendonça Filho, J.G., Menezes, T.R., 2006. Paleoenvironmental reconstruction based on palynofacies analysis of the Aptian–Albian succession of the Sergipe Basin, northeastern Brazil. Marine Micropaleontology 59, 56–81.

Connan, J., Dessort, D., 1987. Novel family of hexacyclic hopanoid alkanes (C_{32}–C_{35}) occurring in sediments and oils from anoxic paleoenvironments. Organic Geochemistry 11, 103–113.

Demaison, G., Holck, A.J.J., Jones, R.W., Moore, G.T., 1983. Predictive source bed stratigraphy; a guide to regional petroleum occurrence–North Sea Basin and eastern North American continental margin. In: Proceedings of the 11th World Petroleum Congress 2. John Wiley & Sons, London, pp. 1–13.

EGPC (Egyptian General Petroleum Corporation) Stratigraphic Committee, 1964. Oligocene and Miocene rock stratigraphy of the Suez region. Egyptian General Petroleum Corporation, Cairo, 142 p.

EGPC (Egyptian General Petroleum Corporation), 1996. Gulf of Suez oil fields (A comprehensive overview). Egyptian General Petroleum Corporation, Cairo, 736 p.

Ekweozor, C.M., Telnaes N., 1990. Oleanane parameter: verification by quantitative study of the biomarker occurrence in sediments of the Niger delta. Organic Geochemistry 16, 401–413.

El Atfy, H., Brocke, R., Uhl, D., 2013a. Age and paleoenvironment of the Nukhul Formation, Gulf of Suez, Egypt: insights from palynology, palynofacies and organic geochemistry. GeoArabia 18, 137–174.

El Atfy, H., Brocke, R., Uhl, D., 2013b. A fungal proliferation near the probable Oligocene/Miocene boundary, Nukhul Formation, Gulf of Suez, Egypt. Journal of Micropalaeontology 32, 183–195.

El Atfy, H., Brocke, R., Uhl, D., Ghassal, B., Stock, A.T., Littke, R., 2014. Source rock potential and paleoenvironment of the Miocene Rudeis and Kareem formations, Gulf of Suez, Egypt: an integrated palynofacies and organic geochemical approach. International Journal of Coal Geology 131, 326–343.

El Ayouty, M.K., 1990. Petroleum Geology. In: Said, R. (Ed.), The Geology of Egypt. A.A. Balkema, Rotterdam, Brookfield, pp. 567–599.

El Beialy, S.Y., Ali, A.S., 2002. Dinoflagellates from the Miocene Rudeis and Kareem formations, borehole GS-78-1, Gulf of Suez, Egypt. Journal of African Earth Sciences 35, 235–245.

El Beialy, S.Y., Mahmoud, M.S., Ali, A.S., 2005. Insights on the age, climate and depositional environments of the Rudeis and Kareem formations, GS-78-1 well, Gulf of Suez, Egypt: a palynological approach. Revista Española de Micropaleontología 37, 273–289.

El Beialy, S.Y., Zobaa, M.K., Taha, A.A., 2016. Depositional paleoenvironment and hydrocarbon source potential of the Oligocene Dabaa Formation, north Western Desert, Egypt: a palynofacies approach. Geosphere 12, 346–353.

El Diasty, W.Sh., Abo Ghonaim, A.A., Mostafa, A.R., El Beialy, S.Y., Edwards, K.J., 2016. Biomarker characteristics of the Turonian–Eocene succession, Belayim oilfields, central Gulf of Suez, Egypt. Journal of the Association of Arab Universities for Basic and Applied Sciences19, 91–100.

El Diasty, W.Sh., El Beialy, S.Y., Abo Ghonaim, A.A., Mostafa, A.R., El Atfy, H., 2014. Palynology, palynofacies and petroleum potential of the Upper Cretaceous–Eocene Matulla, Brown Limestone and Thebes formations, Belayim oilfields, central Gulf of Suez, Egypt. Journal of African Earth Sciences 95, 155–167.

El Diasty, W.Sh., El Beialy, S.Y., Mostafa, A.R., Abo Ghonaim, A.A., Peters, K.E., 2015a. Crude oil geochemistry and source rock potential of the Upper Cretaceous–Eocene succession in the Belayim oilfields, central Gulf of Suez, Egypt. Journal of Petroleum Geology 38, 193–216.

El Diasty, W.Sh., Mostafa, A.R., El Beialy, S.Y., El Adl, H.A., Edwards, K.G., 2015b. Organic geochemical characteristics of the Upper Cretaceous–Early Paleogene source rock and

correlation with some Egyptian mummy bitumen and oil from the southern Gulf of Suez, Egypt. Arabian Journal of Geosciences 8, 9193–9204.

El Diasty, W.Sh., Moldowan, J.M., 2012. Application of biological markers in the recognition of the geochemical characteristics of some crude oils from Abu Gharadig Basin, north Western Desert–Egypt. Marine and Petroleum Geology 35, 28–40.

El Diasty, W.Sh., Peters, K.E., 2014. Genetic classification of oil families in the central and southern sectors, Gulf of Suez, Egypt. Journal of Petroleum Geology 37, 105–126.

Espitalié, J., Laporte, J.L., Madec, M., Marquis, F., Leplat, P., Paulet, J., Boutefeu, A., 1977. Méthode rapide de caractérisation des roches mètres, de leur potential pétrolier et de leur degré d'évolution. Revue de l'Institut Français du Pétrole 32, 23–42.

Evans, A.L., 1988. Neogene tectonic and stratigraphic events in the Gulf of Suez rift area, Egypt. Tectonophysics 153, 235–247.

Hanson, A.D., Zhang, S.C., Moldowan, J.M., Liang, D.G., Zhang, B.M., 2000. Molecular organic geochemistry of the Tarim Basin, northwest China. American Association Petroleum Geologists, Bulletin 84, 1109–1128.

Hughes, G.W., Abdine, S., Girgis, M.H., 1992. Miocene biofacies development and geological history of the Gulf of Suez, Egypt. Marine and Petroleum Geology 9, 2–28.

Hughes, W.B., Holba, A.G., Dzou, L.I.P., 1995. The ratios of dibenzothiophene to phenanthrene and pristane to phytane as indicators of depositional environment and lithology of petroleum source rocks. Geochimica et Cosmochimica Acta 59, 3581–3598.

Hunt, J.M., 1996. Petroleum Geochemistry and Geology, 2nd edition. Freeman, New York, 743 pp.

Mackenzie, A.S., Maxwell, J.R., 1981. Assessment of thermal maturation in sedimentary rocks by molecular measurements. In: Brooks, J. (Ed.), Organic Maturation Studies and Fossil Fuel Exploration. Academic Press, London, pp. 239–254.

Mahmoud, M.S., 1993. Dinocyst stratigraphy of the Middle Miocene from Shagar-1 borehole, SW Gulf of Suez (Egypt). Newsletters on Stratigraphy 28, 79–92.

Mello, M.R., Gaglianone, P.C., Brassell, S.C., Maxwell, J.R., 1988. Geochemical and biological marker assessment of depositional environment using Brazilian offshore oils. Marine and Petroleum Geology 5, 205–203.

Mendonça Filho, J.G., Menezes, T.R., Mendonça, J.O., Oliveira, A.D., Silva, T.F., Rondon, N.F., Silva, F.S., 2012. Organic facies: palynofacies and organic geochemistry approaches. In: Panagiotaras, D. (Ed.), Geochemistry – Earth's System Processes. InTech, Rijeka, pp. 211–248.

Moldowan, J.M., Dahl, J.E., Huizinga, B.J., Taylor, D.W., Hickey, L.J., Peakman, T.M., 1994. The molecular fossil record of oelanane and its relation to angiosperms. Science 265, 768–771.

Moldowan, J.M., Seifert, W.K., Gallegos, E.J., 1985. Relationship between petroleum composition and depositional environment of petroleum source rocks. American Association Petroleum Geologists, Bulletin 69, 1255–1268.

Mostafa, A.R., 1993. Organic geochemistry of source rocks and related crude oils in the Gulf of Suez, Egypt. Berliner Geowissenschaftliche Abhandlungen, Reihe A 147, 163 p.

NSSC (National Stratigraphic Subcommittee), 1976. Miocene rock stratigraphy of Egypt. In: El Gezeery, M.N., Marzouk, I.M. (Eds.), Egyptian Journal of Geology 18. The National Information and Documentation Centre, NIDOC, Cairo, 59 pp. (Imprinted 1974).

Ourisson, G., Albrecht, P., Rohmer, M., 1984. The microbial origin of fossil fuels. Scientific American 251, 44–51.

Palacas, J.G., Donald, E.A., King, J.D., 1984. South Florida Basin – a prime example of carbonate source rocks of petroleum. In: Palacas, J.G. (Ed.), Petroleum Geochemistry and Source Rock Potential of Carbonate Rocks. American Association Petroleum Geologists, Studies in Geology 18, 71–96.

Pearson, M.J., Watkins, D., Pittion, J.L., Caston, D., Small, J.S., 1982. Aspects of burial diagenesis, organic maturation and palaeothermal history of an area in the South Viking Graben, North Sea. In: Brooks, J. (Ed.), Petroleum Geochemistry and Exploration of Europe. Geological Society, London, Special Publication 12, 161–173.

Peters, K.E., Cassa, M.R., 1994. Applied source rock geochemistry. In: Magoon, L.B., Dow, W.G. (Eds.), The Petroleum System – From Source to Trap. American Association of Petroleum Geologists, Memoir 60, 93–120.

Peters, K.E., Moldowan, J.M., 1991. Effects of source, thermal maturity and biodegradation on the distribution and isomerization of homohopanes in petroleum. Organic Geochemistry 17, 47–61.

Peters, K.E., Walters, C.C., Moldowan, J.M., 2005. The Biomarker Guide, 2nd edition. Cambridge University Press, Cambridge, 1155 pp.

Philp, R.P., Gilbert, T.D., 1986. Biomarker distributions in Australian oils predominantly derived from terrigenous source material. Organic Geochemistry 10, 73–84.

Radke, M., Leythaeuser, D., Teichmüller, M., 1984. Relationship between rank and composition of aromatic hydrocarbons for coals of different origins. Organic Geochemistry 6, 423–430.

Rohrback, B.G., 1983. Crude oil geochemistry of the Gulf of Suez. In: Bjorøy, M. et al. (Eds.), Advances in Organic Geochemistry 1981. Wiley, Chichester, pp. 39–48.

Rullkötter, J., Marzi, R., 1988. Natural and artificial maturation of biological markers in a Toarcian shale from northern Germany. Organic Geochemistry 13, 639–645.

Said, R., 1962. The Geology of Egypt. Elsevier, Amsterdam, 377 p.

Said, R., 1990. Cenozoic. In: Said, R. (Ed.), The Geology of Egypt. Balkema, Rotterdam, Brookfield, pp. 567–599.

Schlumberger, 1984. Well Evaluation Conference, Egypt. In: Smith, Ch.M. (Ed.), 64 p.

Scott, R.W., Govean, F.M., 1985. Early depositional history of a rift basin: Miocene in Western Sinai. Palaeogeography, Palaeoclimatololgy, Palaeoecology 52, 143–158.

Seifert, W.K., Moldowan, J.M., 1986. Use of biological markers in petroleum exploration. In: Johns, R.B. (Ed.), Biological Markers in the Sedimentary Record. Methods in Geochemistry and Geophysics 24, 261–290.

Sinninghe Damsté, J.S., Kenig, F., Koopmans, M.P., Köster, J., Schouten, S., Hayes, J.M., de Leeuw, J.W., 1995. Evidence for gammacerane as an indicator of water column stratification. Geochimica et Cosmochimica Acta 59, 1895–1900.

Smale, J.L., Thunell, R.C., Schamel, S., 1988. Sedimentological evidence for early Miocene fault reactivation in the Gulf of Suez. Geology 16, 113–116.

Sofer, Z., 1984. Stable carbon isotope compositions of crude oils: application to source depositional environments and petroleum alteration. American Association of Petroleum Geologists, Bulletin 68, 31–49.

Soliman, A., Ćorić, S., Head, M.J., Piller, W.E., El Beialy, S.Y., 2012. Lower and middle Miocene biostratigraphy, Gulf of Suez, Egypt based on dinoflagellate cysts and calcareous nannofossils. Palynology 36, 38–79.

Soliman, A., Ibrahim, M., 2012. Dinoflagellate cyst stratigraphy and paleoenvironment of the Lower and Middle Miocene, Gulf of Suez, Egypt. Egyptian Journal of Paleontology 12, 97–122.

ten Haven, H.L., Rohmer, M., Rullkötter, J., Bisseret, P., 1989. Tetrahymanol, the most likely precursor of gammacerane, occurs ubiquitously in marine sediments. Geochimica et Cosmochimica Acta 53, 3073–3079.

Thompson, C.L., Dembicki, H.J., 1986. Optical characteristics of amorphous kerogens and the hydrocarbon-generating potential of source rocks. International Journal of Coal Geology 6, 229–249.

Traverse, A. 2007. Paleopalynology, 2nd edition. Springer, Dordrecht, 813 p.

Tyson, R.V., 1993. Palynofacies analysis. In: Jenkins, D.G. (Ed.), Applied Micropaleontology. Kluwer, Dordrecht, pp. 153–191.

Tyson, R.V., 1995. Sedimentary Organic Matter – Organic Facies and Palynofacies. Chapman and Hall, London, 615 p.

Volk, H., George, C.S., Middleton, H., Schofield, S., 2005. Geochemical comparison of fluid inclusion and present-day oil accumulations in the Papuan Foreland, evidence for previously unrecognised petroleum source rocks. Organic Geochemistry 36, 29–51.

Zumberge, J.E., 1987. Prediction of source rock characteristics based on terpane biomarkers in crude oils: a multivariate statistical approach, Geochimica et Cosmochimica Acta 51, 1625–1637.

Figure captions

Fig. 1. Location maps, lithostratigraphic correlation of, and sampling horizons for, the four wells in the Ras El Bahar Oilfield examined in this study.

Fig. 2. Generalized lithostratigraphic column for the study area in the southwestern Gulf of Suez, with petroleum system elements (compiled after Alsharhan, 2003 and El Atfy et al., 2014). Tort, Tortonian; Mess, Messinian; Aquit, Aquitanian; Turon, Turonian; Cenom, Cenomanian; Mhei, Mheiherrat; Haw, Hawara; Ghar, Gharmul; Oct, October; Gha, Ghara; Abu Ze, Abu Zenima.

Fig. 3. Plot of total organic carbon (TOC, wt%) versus the hydrocarbons remaining in the rock (S_1 mg HC/g rock) plus the remaining hydrocarbon potential within the rock (S_2 mg HC/g rock), showing mostly fair to good petroleum-generating potential for the rock units examined.

Fig. 4. Modified van Krevelen diagram of hydrogen versus oxygen indexes showing kerogen type and hydrocarbon generation potential of the rocks examined.

Fig. 5. Ternary plot (modified after Tyson, 1993) showing AOM, phytoclast and palynomorph data from the Upper Cretaceous–Miocene succession.

Fig. 6. Relative abundance of the major palynofacies components plotted against depth in the formations penetrated by the Ras El Bahar-2 well.

Fig. 7. Integrated organic geochemical parameters (TOC, S_2, HI) and palynofacies components (AOM and phytoclasts) versus depth for the samples analyzed.

Fig. 8. Transmitted light photographs of components of the palynofacies from the Ras El Bahar Oilfield. For each of these the combined well name, sample number and slide reference (e.g., RB4.3a) is followed by the depth (in m) of the horizon sampled and an England Finder reference. Magnifications are indicated by scale bars. A, light brown, angular to sub-angular, finely divided and aggregated AOM; RB5.7a, 1980 m, N37-3. B, cuticle; RB5.7a, 1980m, J44. C, D, other tissues: C, RB4.4a, 1700 m, N50; D, RB5.4a, 1920 m, G44-3. E–J, dinoflagellate cysts. E, *Sumatradinium*

sp. cf. *S. hispidum*; RB4.3b, 1668 m, R39-3. F, *Cordosphaeridium minimum*; RB4.6a, 1767 m, G34. G, H, *Spiniferites* sp. cf. *S. pseudofurcatus*: RB1.2a, 1422 m, L39-2; RB 5.2a, 1887 m, D42-3. I, *Spiniferites* sp. cf. *S. ramosus*; RB4.5a, 1752 m, R55. J, *Melitasphaeridium choanophorum*; RB4.3a, 1668 m, S46-4.

Fig. 9. Transmitted light photographs of components of the palynofacies from the Ras El Bahar Oilfield: accompanying data as for Fig. 8. A, an assemblage of granular AOM with remains of internal structures and a monolete spore (red arrow); RB2.12a, 2367 m, L43-3. B, light brown AOM and *Polysphaeridium* sp. (red arrow); RB2.13a, 2409 m, H41. C, *Stephanocolpites* sp.; RB2.8a, 2211 m, R53-4. D, *Selenopemphix brevispinosa*; RB2.5a, 2133 m, J50-3. E, *Polysphaeridium* sp.; RB2.13a, 2409 m, H41-2.

Fig. 10. Transmitted light photographs of components of the palynofacies from the Ras El Bahar Oilfield: accompanying data as for Fig. 8. A, non-marine AOM of clotted appearance in association with over-mature amorphous particles; RB2.18a, 2652 m, T34. B, marine AOM; RB2.15a, 2514 m, B54. C, fungal spore; RB2.20a, 2703 m, L46-1. D, *Ephedripites* sp.; RB2.15a, 2514 m, Q52. E, *Phragmothyrites* sp.; RB4.6a, 1767 m, M35-3.

Fig. 11. Examples of GC-MS mass chromatograms for the Cretaceous–Miocene rock extracts analyzed.

Fig. 12. Plot of C_{22}/C_{21} and C_{24}/C_{23} tricyclic terpanes to predict depositional environments of the Upper Cretaceous–Miocene samples in the study area.

Fig. 13. Plot of T_{max} (maximum temperature) versus PI (production index) showing the level of maturation and nature of hydrocarbon products of the Upper Cretaceous–Miocene samples examined.

Fig. 14. Cross-plot of two biomarker parameters sensitive to thermal maturity from the Wata, Esna, Rudeis and Kareem deposits in the Ras El Bahar Oilfield.

Table captions

Table 1. Bulk geochemical results of Rock-Eval/TOC analysis with calculated parameters for cuttings samples from the Ras El Bahar Oilfield.

Table 2. Distribution of the palynomorphs encountered in the palynofacies from the Upper Cretaceous–Miocene formations in the Ras El Bahar Oilfield.

Table 3. Quantitative distribution of various palynofacies particles recorded from the formations examined.

Table 4. Geological data, carbon isotopes, hopane, sterane and aromatic values calculated for selected source rock extracts.

Figure 1

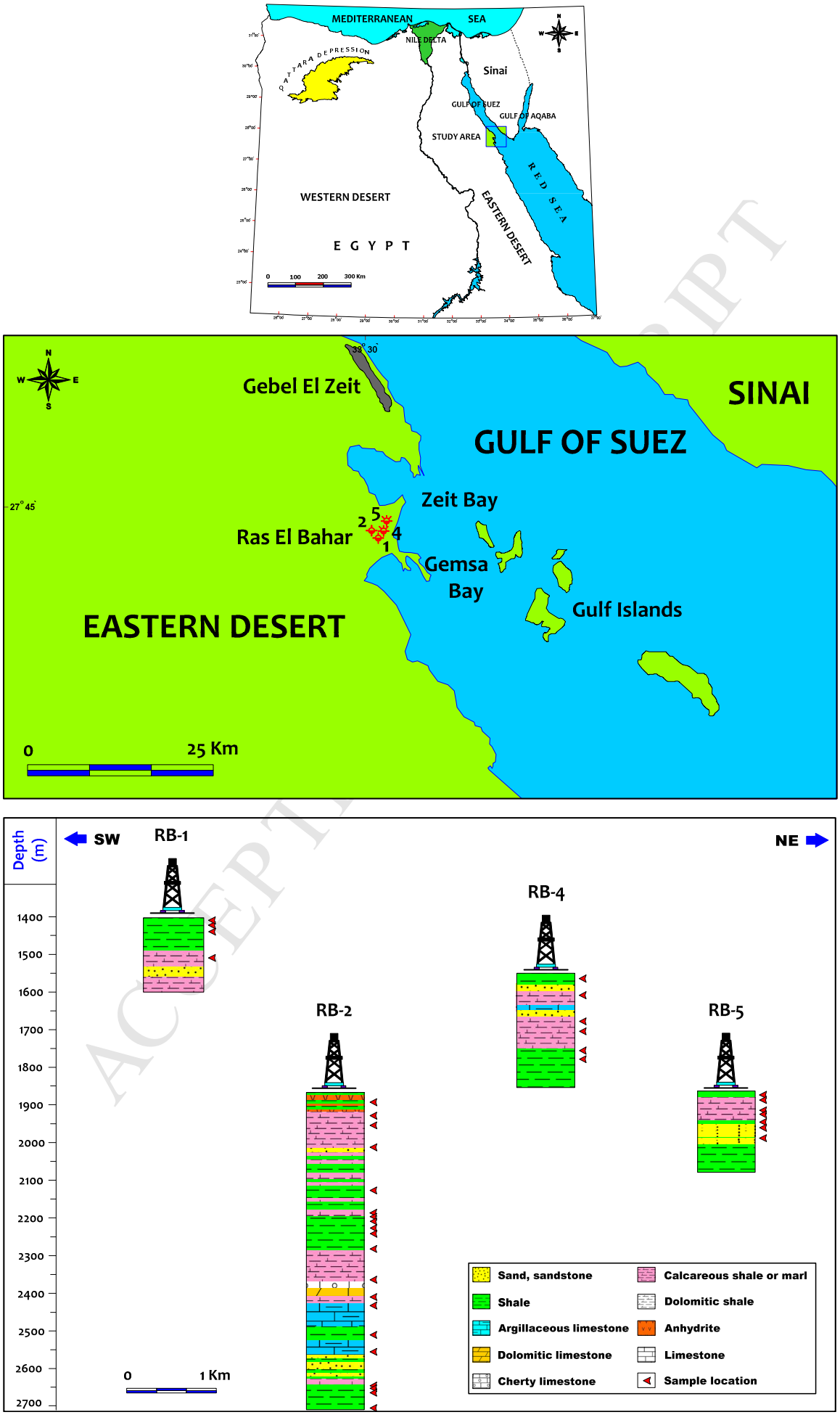
MEDITERRANEAN SEA
NILE DELTA
QATTARA DEPRESSION
Sinai
GULF OF SUEZ
GULF OF AQABA
STUDY AREA
RED SEA
WESTERN DESERT
EASTERN DESERT
E G Y P T
0 100 200 300 Km
N
W
E
S
38° 30'
Gebel El Zeit
SINAI
GULF OF SUEZ
Zeit Bay
27° 45'
Ras El Bahar
1
2
4
5
Gemsa Bay
Gulf Islands
EASTERN DESERT
0 25 Km
Depth (m)
SW
NE
RB-1
RB-2
RB-4
RB-5
1400
1500
1600
1700
1800
1900
2000
2100
2200
2300
2400
2500
2600
2700
0 1 Km
Sand, sandstone
Shale
Argillaceous limestone
Dolomitic limestone
Cherty limestone
Calcareous shale or marl
Dolomitic shale
Anhydrite
Limestone
Sample location

Figure 2

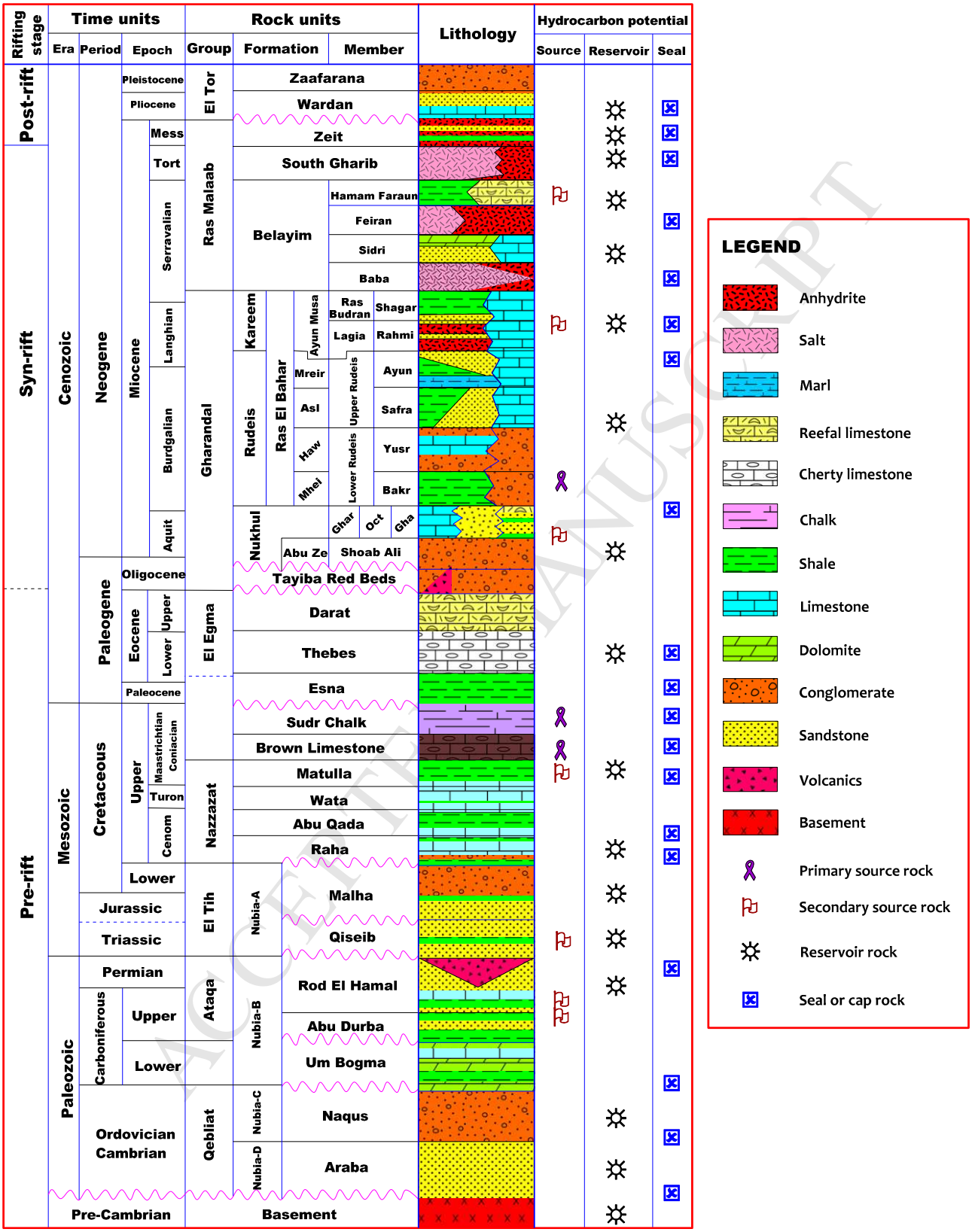

Figure 3

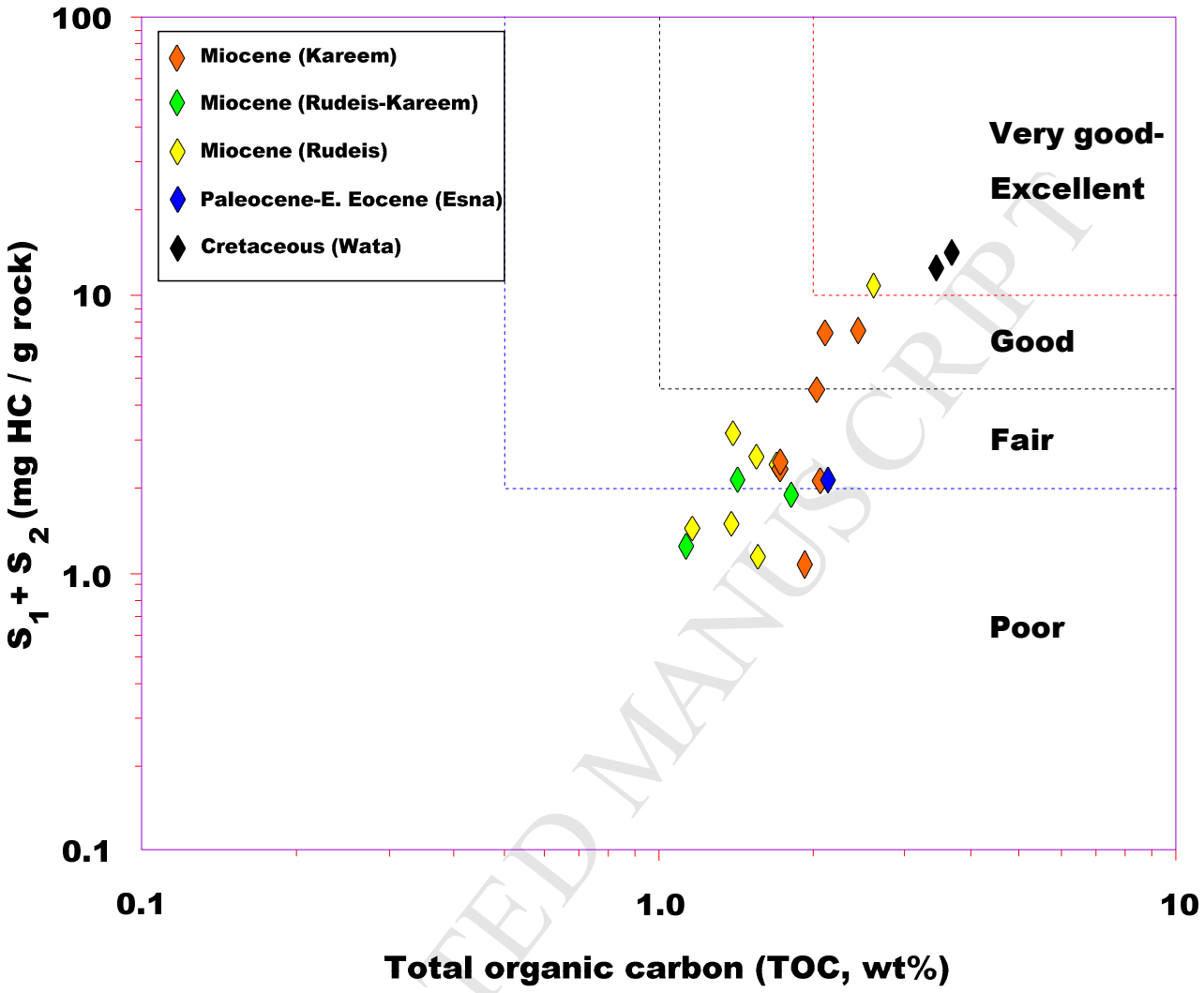

Figure 4

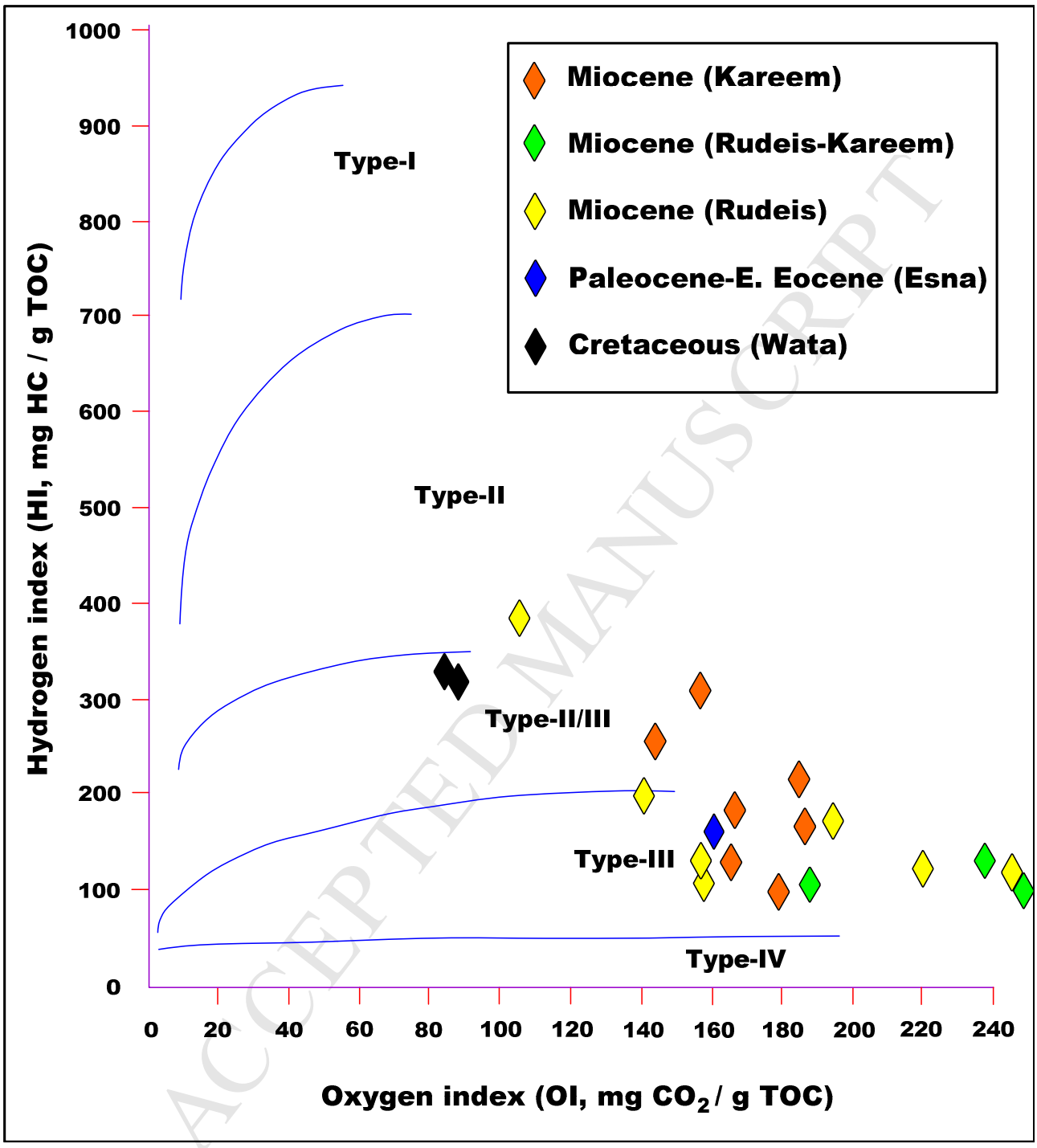

Figure 5

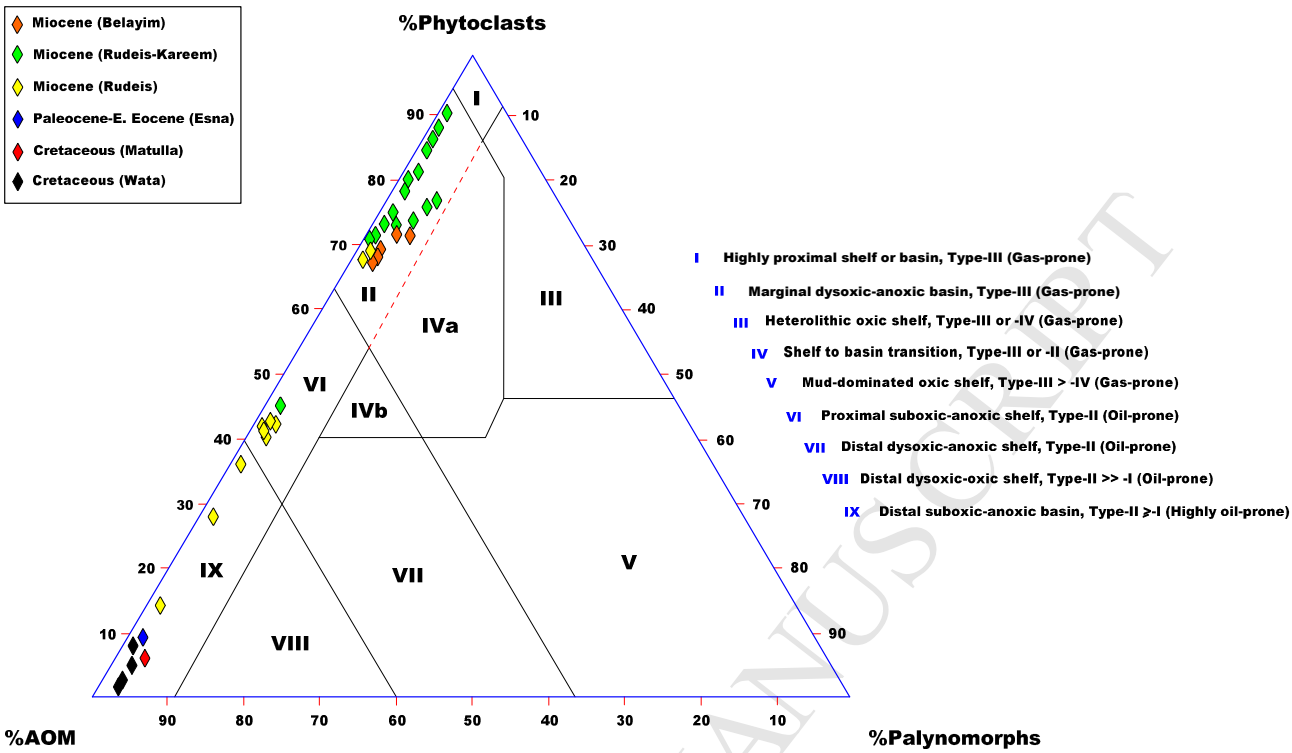

Figure 6

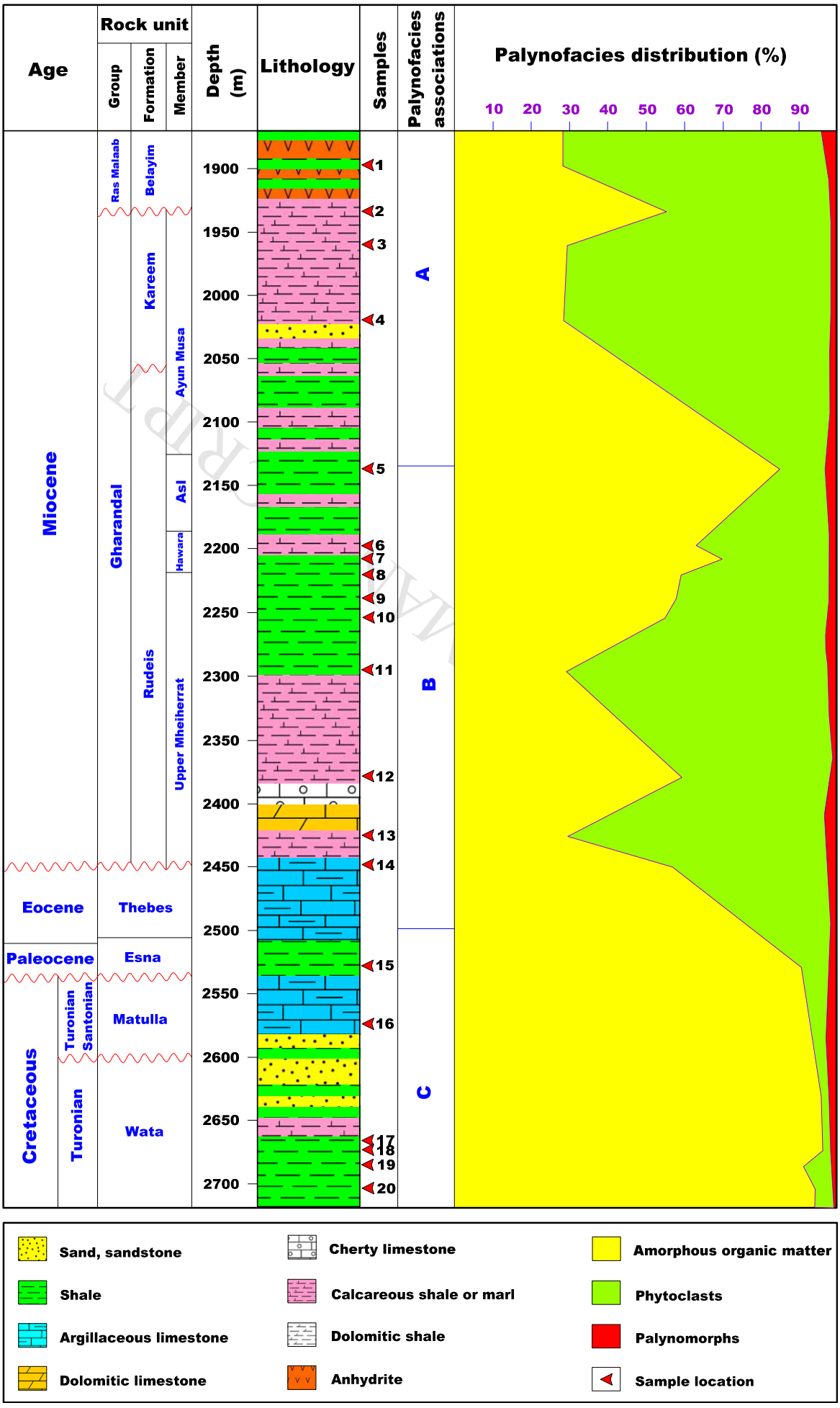

Figure 7

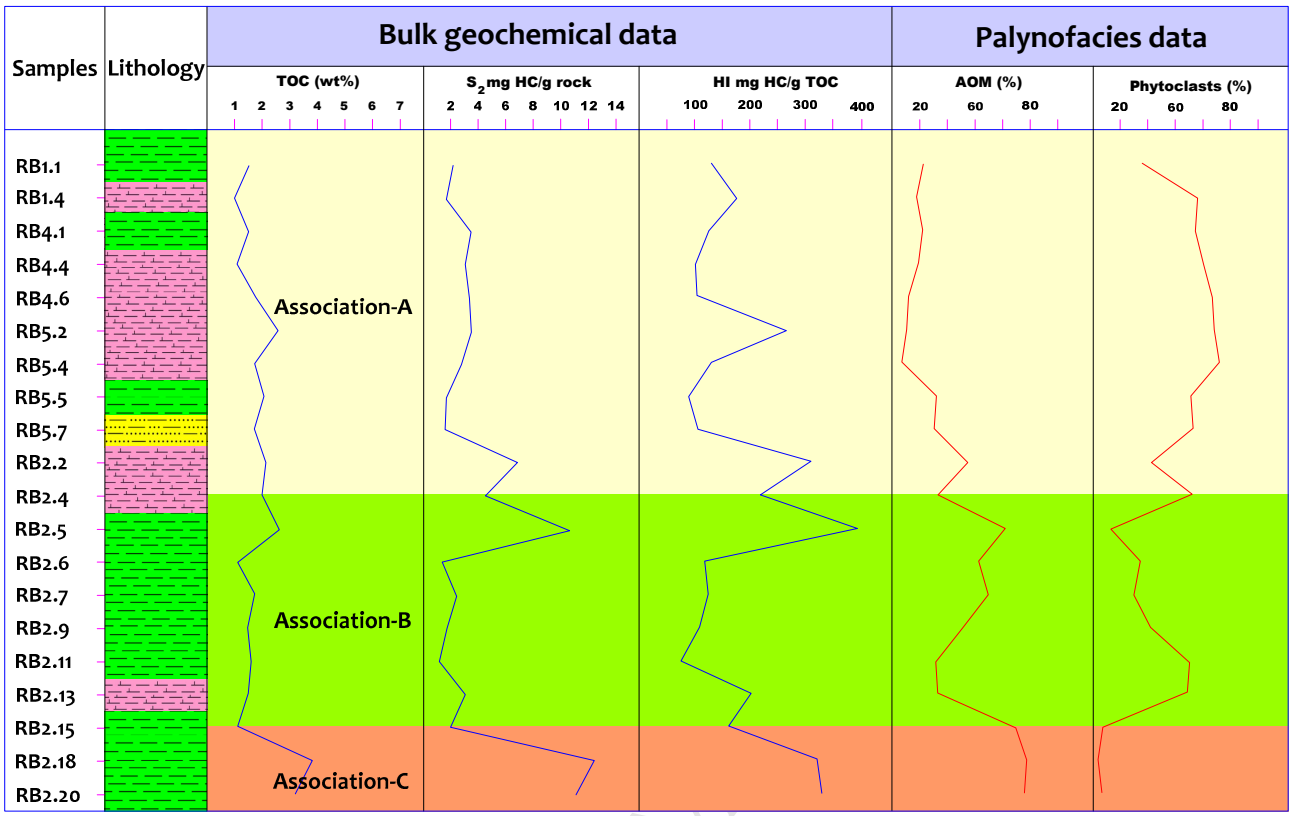

Figure 8

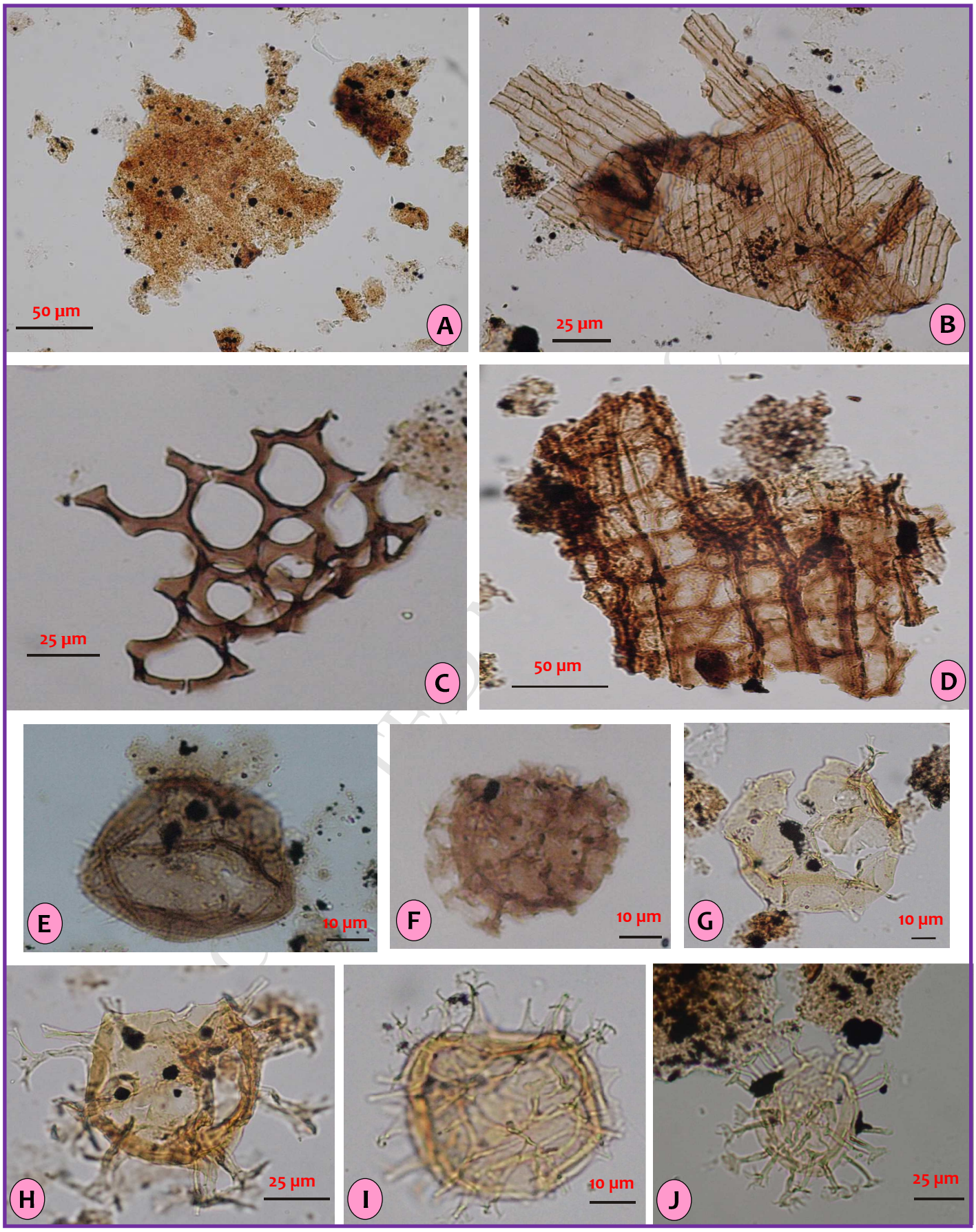
50 µm
A
25 µm
B
25 µm
C
50 µm
D
E
10 µm
F
10 µm
G
10 µm
H
25 µm
I
10 µm
J
25 µm

Figure 9

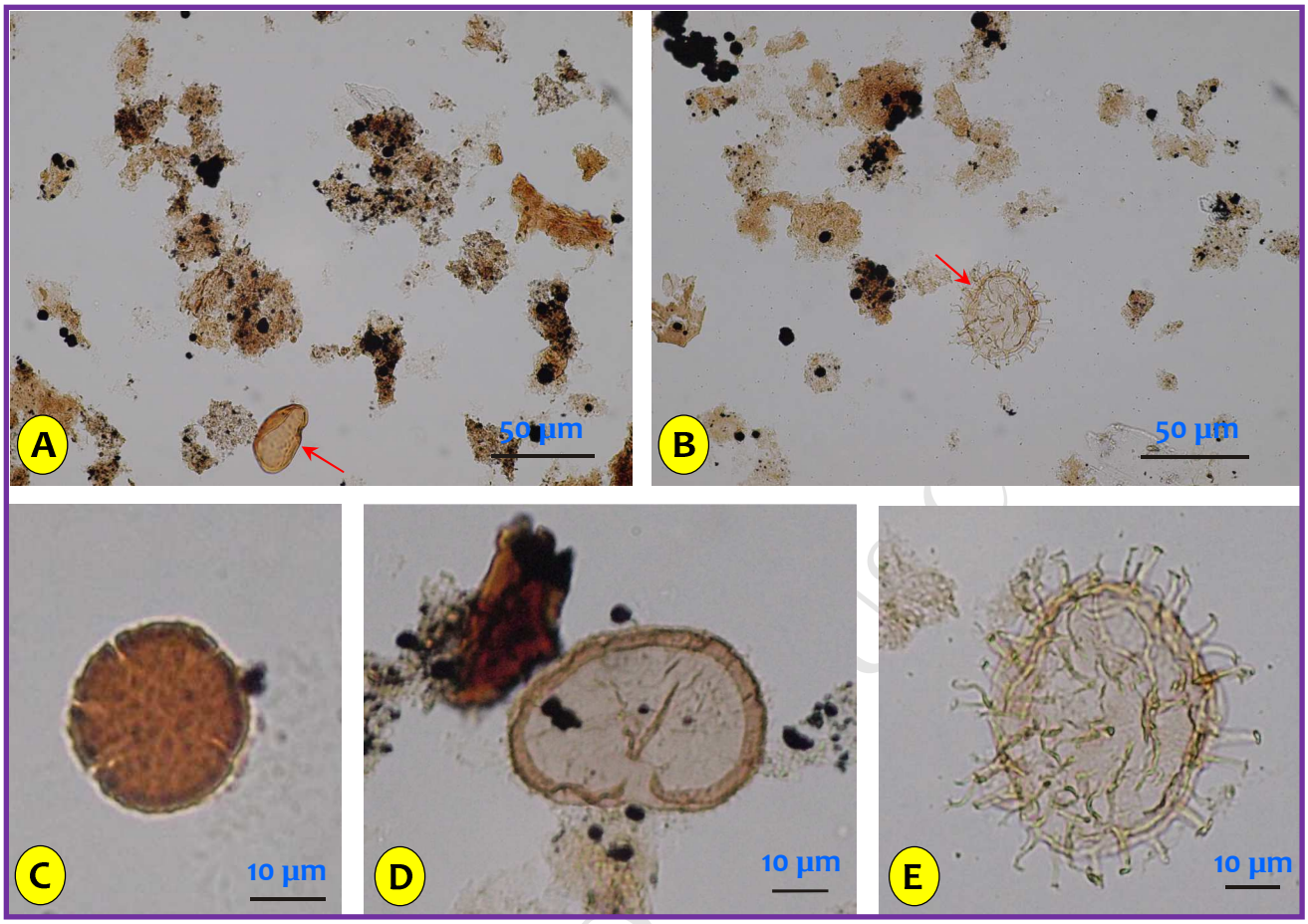

Figure 10

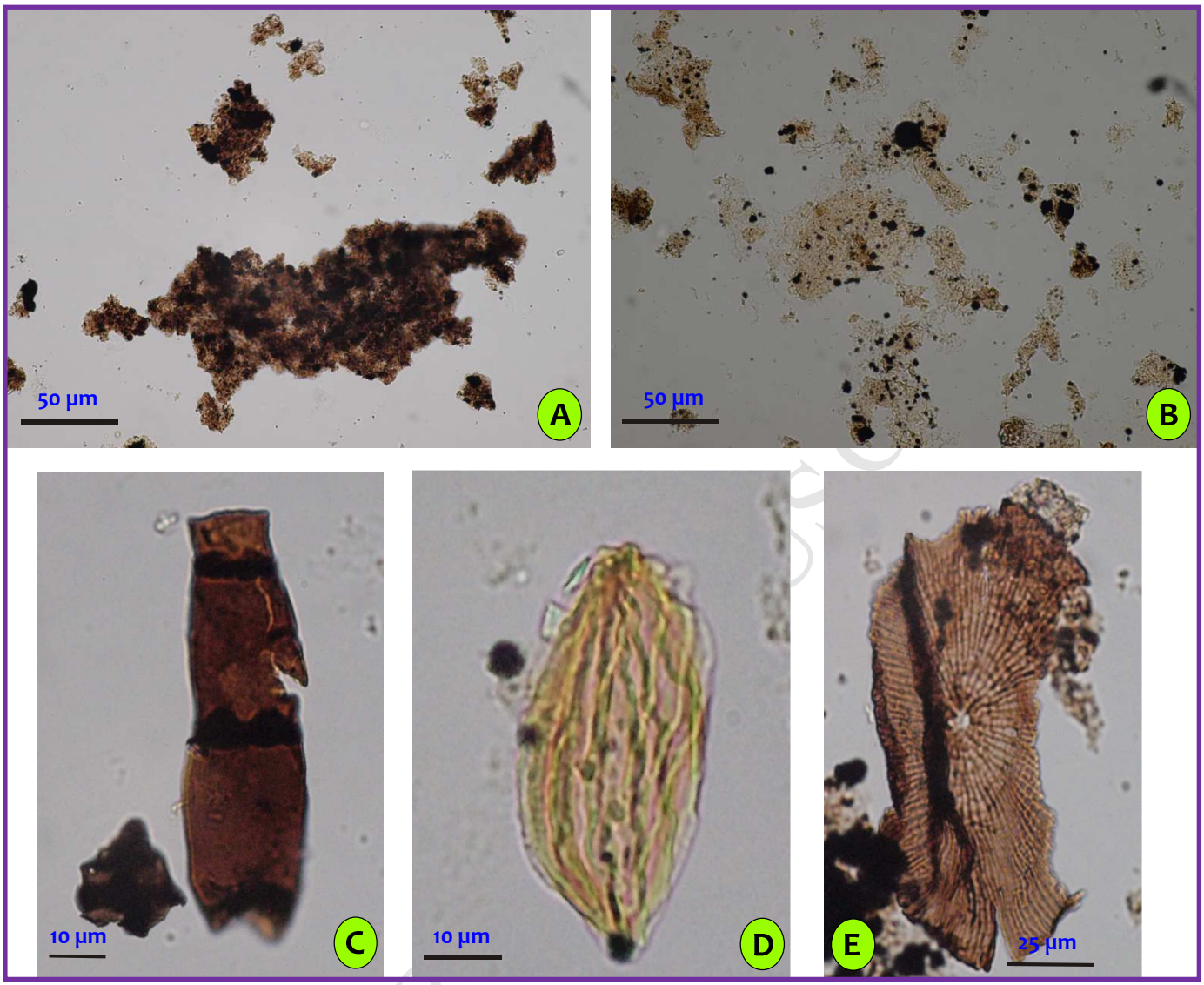

Figure 11

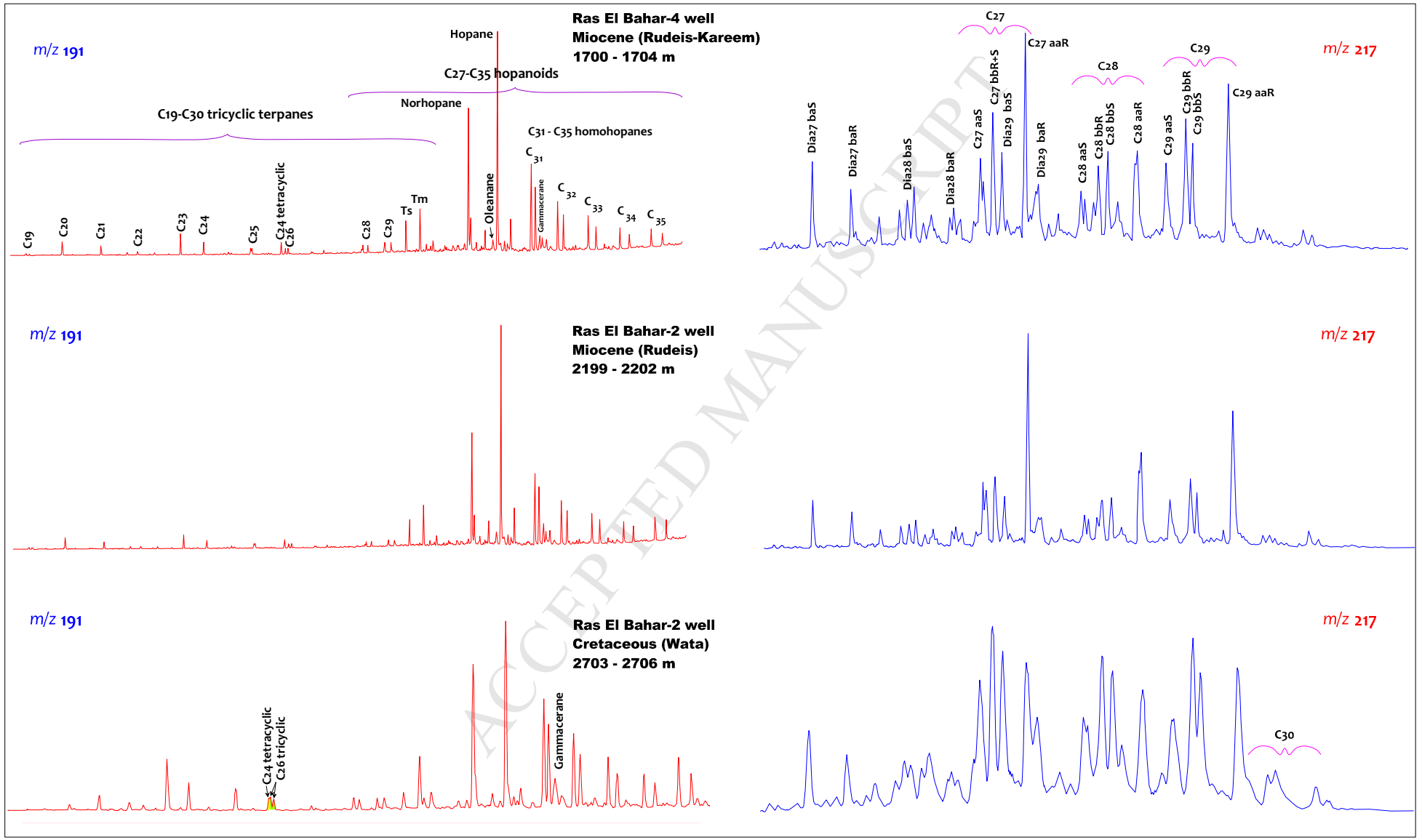

Figure 12

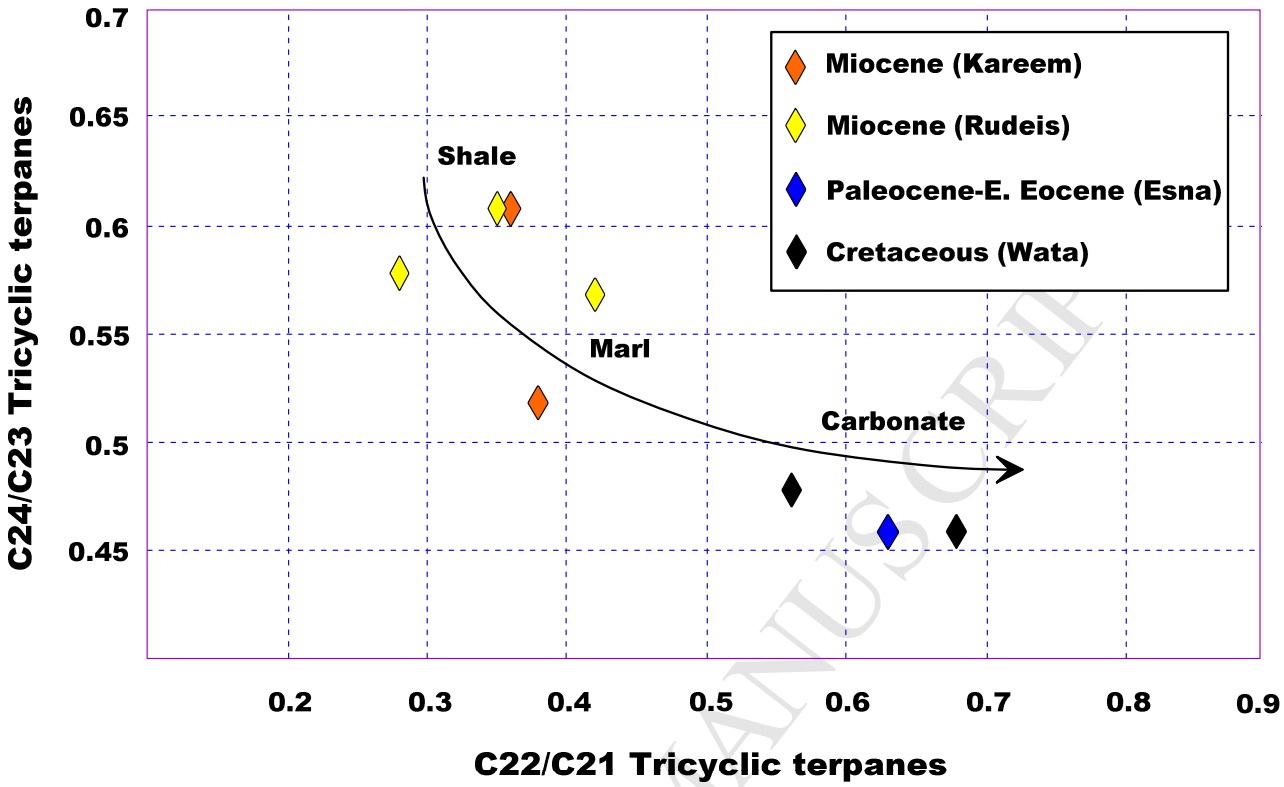

Figure 13

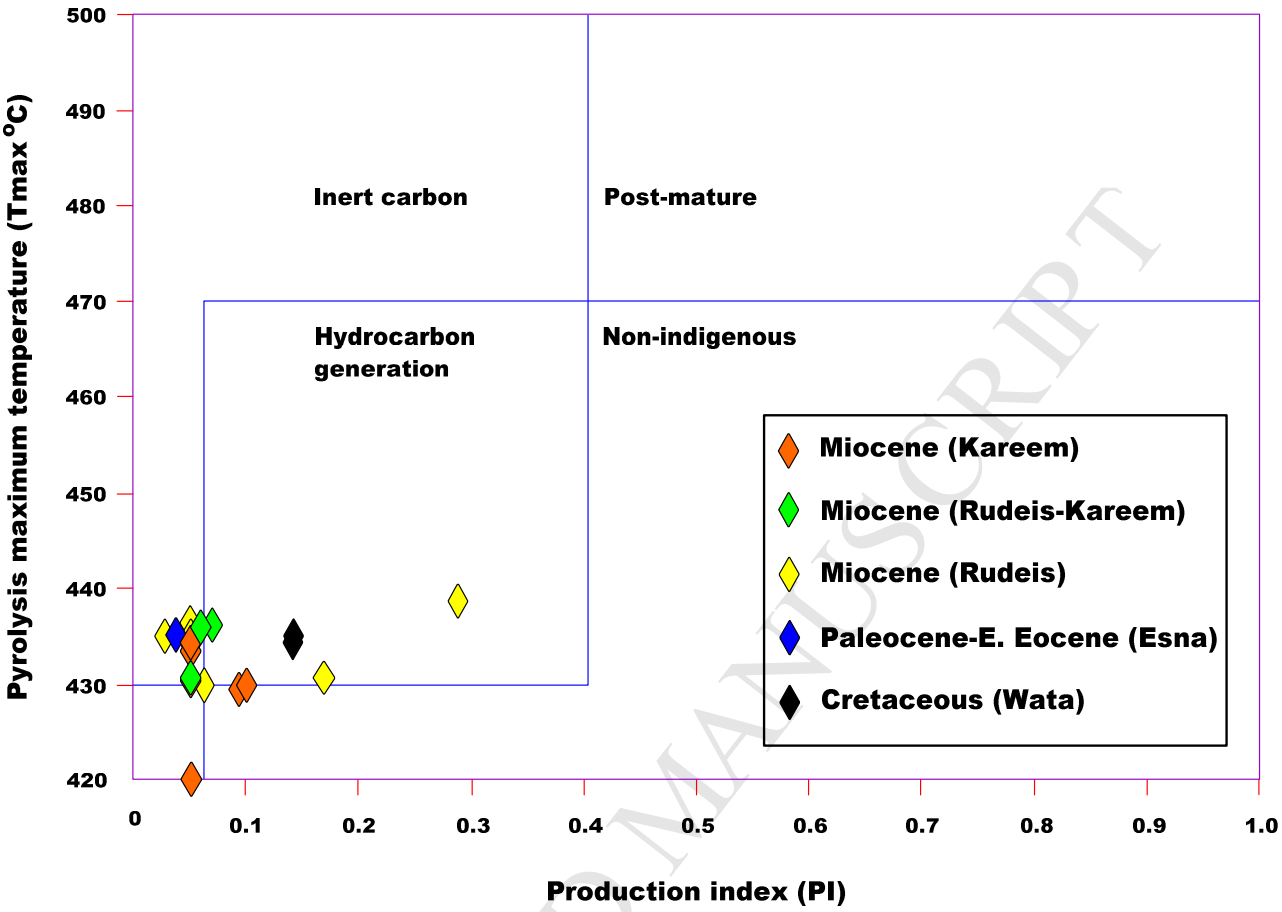

Figure 14

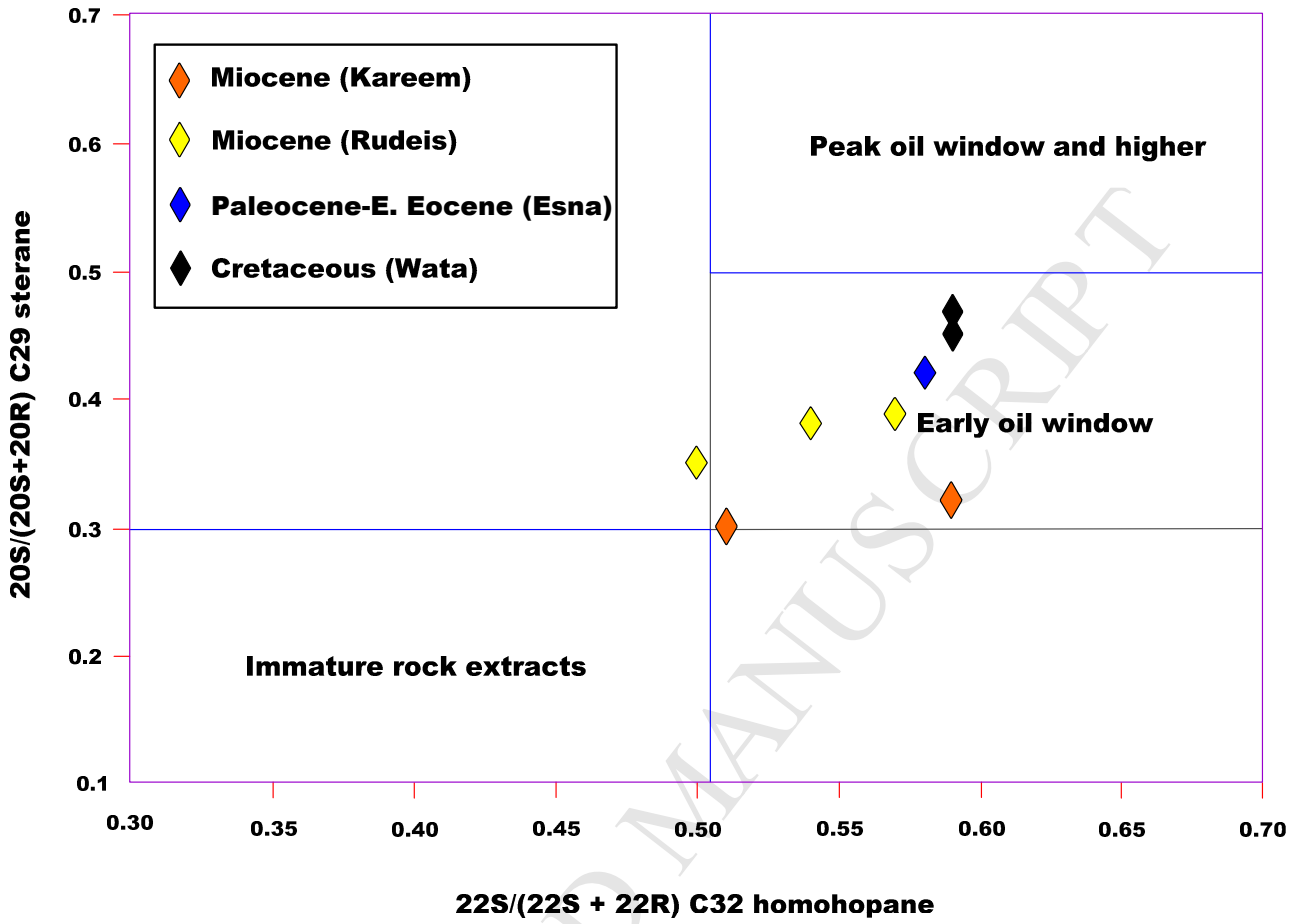

Table 1

Sample ID	Depth (m)	Lithology	Formation	Age	Petroleum potential (quantity)				Kerogen type (quality)				Thermal maturity	
					TOC (wt %)	S_1 mg/g	S_2 mg/g	S_3 mg/g	HI mg/g	OI mg/g	S_2/S_3	Kerogen type	T_{max} (°C)	PI
RB1.1	1407–1410	Shale	Rudeis	Miocene	1.59	0.46	2.15	2.50	135	157	0.86	III	431	0. 17
RB1.4	1506–1509	Marl	Kareem	Miocene	1.06	0.08	1.83	1.97	172	186	1.02	III	433	0.04
RB2.2	1932–1935	Calcareous shale	Kareem	Miocene	2.19	0.30	6.80	3.41	310	156	1.99	II/III	416	0.04
RB2.4	2016–2019	Calcareous shale	Kareem	Miocene	2.02	0.25	4.40	3.71	218	184	1.19	II/III	432	0.05
RB2.5	2133–2136	Shale	Rudeis	Miocene	2.65	0.72	10.31	2.81	389	106	3.67	II	430	0.06
RB2.6	2178–2181	Shale	Rudeis	Miocene	1.20	0.05	1.45	3.00	121	250	0.48	III	437	0.04
RB2.7	2199–2202	Shale	Rudeis	Miocene	1.76	0.11	2.22	3.88	126	220	0.57	III	434	0.04
RB2.9	2229–2232	Shale	Rudeis	Miocene	1.48	0.01	1.63	2.34	110	158	0.70	III	435	0.01
RB2.11	2286–2289	Shale	Rudeis	Miocene	1.58	0.03	1.19	3.09	175	195	0.39	III	438	0.28
RB2.13	2409–2412	Marl	Rudeis	Miocene	1.49	0.15	3.00	2.10	201	141	1.43	II/III	435	0.04
RB2.15	2514–2517	Shale	Esna	Paleocene-Early Eocene	1.19	0.06	1.96	1.92	165	161	1.02	III	435	0.03
RB2.18	2652–2655	Shale	Wata	Cretaceous	3.80	1.85	12.29	3.35	323	88	3.67	II/III	434	0.13
RB2.20	2703–2706	Shale	Wata	Cretaceous	3.34	1.68	11.00	2.80	329	84	3.93	II/III	435	0.13
RB4.1	1560–1563	Shale	Rudeis–Kareem	Miocene	1.51	0.08	1.97	3.60	130	238	0.55	III	431	0.04
RB4.4	1700–1704	Marl	Rudeis–Kareem	Miocene	1.20	0.09	1.20	3.05	100	254	0.39	III	437	0.06
RB4.6	1767–1770	Shale	Rudeis–Kareem	Miocene	1.76	0.10	1.87	3.31	106	188	0.56	III	436	0.05
RB5.2	1887–1890	Marl	Kareem	Miocene	2.55	0.68	6.66	3.64	261	143	1.83	II/III	429	0.09
RB5.4	1920–1923	Calcareous shale	Kareem	Miocene	1.75	0.12	2.32	2.88	133	165	0.81	III	434	0.04
RB5.5	1947–1950	Shale	Kareem	Miocene	2.11	0.21	1.85	3.51	188	166	0.53	III	430	0.10
RB5.7	1980–1982	Sandy shale	Kareem	Miocene	1.75	1.75	1.78	3.11	102	178	0.57	III	431	0.04

TOC = Total organic carbon as weight percent organic carbon in rock; **S_1** = Free hydrocarbons emitted from rock without cracking of kerogen (mg hydrocarbons per gram of rock); **S_2** = Residual hydrocarbons representing the remaining generative hydrocarbon potential (mg hydrocarbons per gram of rock); **S_3** = Generated carbon dioxide (mg carbon dioxide per gram of rock); **HI** = Hydrogen index = $S_2 \times 100/TOC$; **OI** = Oxygen index = $S_3 \times 100/TOC$; **T_{max}** = Temperature reached during maximum generation of hydrocarbons measured via S_2 peak of Rock-Eval pyrolysis (°C); **PI** = Production index = $S_1/(S_1+S_2)$.

Table 2

Well name	Sample ID	Depth (m)	Age	Formation	Palynomorphs							
					Spores	Pollen	Dinoflagellates		Acrit-archs	Fungal spores	Forams	Total count
							Peridini-oids	Gonyaulac-oids				
Ras El Bahar-1	RB1.1	1407–10	Miocene	Belayim	0	2	0	0	0	3	0	5
	RB1.2	1422–25	Miocene	Belayim	1	4	2	8	6	7	0	28
	RB1.3	1440–43	Miocene	Belayim	0	0	0	0	3	4	0	7
	RB1.4	1506–09	Miocene	Belayim	1	5	0	3	1	5	0	15
Ras El Bahar-2	RB2.1	1893–96	Miocene	Belayim	3	2	0	0	0	1	0	6
	RB2.2	1932–35	Miocene	Rudeis–Kareem	1	0	0	1	0	1	0	3
	RB2.3	1953–56	Miocene		0	1	0	1	2	0	0	4
	RB2.4	2016–19	Miocene		0	0	1	0	0	1	0	2
	RB2.5	2133–36	Miocene	Rudeis	1	0	0	0	1	0	0	2
	RB2.6	2178–81	Miocene		0	2	0	1	1	1	0	5
	RB2.7	2199–02	Miocene		0	5	0	1	1	0	0	7
	RB2.8	2211–14	Miocene		0	0	0	2	1	1	0	4
	RB2.9	2229–32	Miocene		0	1	0	0	0	1	0	2
	RB2.10	2244–47	Miocene		0	2	1	0	1	1	0	5
	RB2.11	2286–89	Miocene		1	1	0	0	0	1	0	3
	RB2.12	2367–70	Miocene		0	0	0	1	0	0	1	2
	RB2.13	2409–12	Miocene		1	1	0	2	0	1	0	5
	RB2.14	2436–39	Miocene		0	3	0	1	0	0	1	5
	RB2.15	2514–17	Paleocene-Early Eocene	Esna	0	1	0	0	1	1	0	3
	RB2.16	2556–59	Turonian-Santonian	Matulla	1	1	0	0	0	1	0	3
	RB2.17	2643–46	Turonian	Wata	0	1	0	1	0	2	0	4
	RB2.18	2652–55	Turonian		2	1	0	0	0	0	0	3
	RB2.19	2664–67	Turonian		0	1	0	0	0	1	1	3
	RB2.20	2703–06	Turonian		0	1	0	0	1	1	0	3
Ras El Bahar-4	RB4.1	1560–63	Miocene	Rudeis–Kareem	0	2	0	2	0	0	0	4
	RB4.2	1605–08	Miocene		0	3	0	0	1	2	1	7
	RB4.3	1668–71	Miocene		0	3	0	4	0	0	0	7
	RB4.4	1700–04	Miocene		3	6	1	5	0	3	1	19
	RB4.5	1752–55	Miocene		7	3	0	22	2	0	2	36
	RB4.6	1767–70	Miocene		0	6	0	5	2	2	2	17
Ras El Bahar-5	RB5.1	1869–72	Miocene	Rudeis–Kareem	1	2	0	2	0	0	0	5
	RB5.2	1887–90	Miocene		0	0	0	3	0	0	1	4
	RB5.3	1914–17	Miocene		0	1	0	3	1	1	0	6
	RB5.4	1920–23	Miocene		1	1	0	0	1	0	0	3
	RB5.5	1947–50	Miocene		1	0	0	2	1	0	1	5
	RB5.6	1953–56	Miocene		2	2	0	0	1	0	0	5
	RB5.7	1980–82	Miocene		0	1	0	0	1	0	1	3

Table 3

Well name	Sample ID	Depth (m)	Age	Formation	Member	Lithology	Palynofacies association	Palynofacies distribution (%)		
			(EGPC, 1964)					AOM	Phytoclasts	Plyno-morphs
Ras El Bahar-1	RB1.1	1407–1410	Miocene	Belayim		Shale	A	28	70	2
	RB1.2	1422–1425				Shale		23	71	6
	RB1.3	1440–1443				Shale		29	68	3
	RB1.4	1506–1509				Marl		24	72	4
Ras El Bahar-2	RB2.1	1893–1896	Miocene	Belayim		Shale	A	28	69	3
	RB2.2	1932–1935		Rudeis–Kareem	Ayun Musa	Calc. shale		55	44	1
	RB2.3	1953–1956				Calc. shale		29	70	1
	RB2.4	2016–2019				Calc. shale		28	71	1
	RB2.5	2133–2136		Rudeis	Asl	Shale	B	85	14	1
	RB2.6	2178–2181				Marl		63	36	1
	RB2.7	2199–2202			Hawara	Shale		70	28	2
	RB2.8	2211–2214				Shale		58	41	1
	RB2.9	2229–2232			Upper Mheiherrat	Shale		57	42	1
	RB2.10	2244–2247				Shale		55	43	2
	RB2.11	2286–2289				Shale		29	70	1
	RB2.12	2367–2370				Marl		59	41	0
	RB2.13	2409–2412				Marl		29	69	2
	RB2.14	2436–2439				Arg. limestone		57	42	1
	RB2.15	2514–2517	Paleocene–Early Eocene	Esna		Shale	C	90	9	1
	RB2.16	2556–2559	Turonian–Santonian	Matulla		Arg. limestone		93	6	1
	RB2.17	2643–2646	Turonian	Wata		Shale		97	1	2
	RB2.18	2652–2655				Shale		97	2	1
	RB2.19	2664–2667				Shale		91	8	1
	RB2.20	2703–2706				Shale		94	5	1
Ras El Bahar-4	RB4.1	1560–1563	Miocene	Rudeis–Kareem	Ayun Musa	Shale	A	25	73	2
	RB4.2	1605–1608				Marl		23	75	2
	RB4.3	1668–1671				Marl		24	73	3
	RB4.4	1700–1704				Marl		18	76	6
	RB4.5	1752–1755				Shale		16	77	7
	RB4.6	1767–1770				Shale		21	74	5
Ras El Bahar-5	RB5.1	1869–1872	Miocene	Rudeis–Kareem		Shale	A	20	78	2
	RB5.2	1887–1890				Marl		19	80	1
	RB5.3	1914–1917				Calc. shale		17	81	2
	RB5.4	1920–1923				Calc. shale		14	85	1
	RB5.5	1947–1950				Shale		12	87	1
	RB5.6	1953–1956				Sandy shale		11	88	1
	RB5.7	1980–1982				Sandy shale		8	91	1

Table 4

Parameter	RB4.4	RB5.1	RB2.6	RB2.7	RB2.12	RB2.15	RB2.18	RB2.20
Geologic data								
Depth (m)	1700–1704	1869–1872	2178–2181	2199–2202	2367–2370	2520–2529	2652–2655	2703–2706
Age	Miocene	Miocene	Miocene	Miocene	Miocene	Paleocene–Early Eocene	Cretaceous	Cretaceous
Formation	Rudeis–Kareem	Kareem	Rudeis	Rudeis	Rudeis	Esna	Wata	Wata
Carbon isotope data								
$\delta^{13}C_{saturates}$	-28.13	-26.67	-27.99	-27.60	-28.26	–	–	–
$\delta^{13}C_{aromatics}$	-27.80	-25.32	-27.26	-26.85	-27.81	–	–	–
CV	-2.20	-0.39	-1.35	-1.43	-1.89	–	–	–
Terpane (*m/z* 191)								
C_{19}/C_{23}	0.09	0.05	0.09	0.12	0.16	0.04	0.04	0.06
C_{22}/C_{21}	0.36	0.38	0.42	0.35	0.28	0.63	0.56	0.68
C_{24}/C_{23}	0.61	0.52	0.57	0.61	0.58	0.46	0.48	0.46
C_{25}/C_{26}	1.05	1.19	1.20	1.03	0.94	1.26	1.49	1.20
Tet/C_{26}	1.00	1.00	1.50	1.00	1.00	0.59	0.65	0.52
C_{27} Ts/Tm	0.73	0.73	0.64	0.67	0.46	0.36	0.35	0.36
C_{29}/H	0.65	0.38	0.55	0.51	0.62	0.64	0.62	0.72
OL/H	0.05	0.08	0.06	0.05	0.13	0.00	0.00	0.00
C_{31}R/H	0.29	0.21	0.28	0.26	0.30	0.41	0.39	0.44
GA/H	0.09	0.60	0.13	0.10	0.09	0.31	0.32	0.27
$C_{35}S/C_{34}S$	0.84	2.67	1.17	1.08	1.09	1.39	1.40	1.45
S/H	0.41	3.04	0.74	0.62	0.58	0.54	0.61	0.47
% $C_{32}S$	0.59	0.51	0.54	0.57	0.50	0.58	0.59	0.59
Sterane (*m/z* 217)								
%C_{27}	32.05	50.47	35.02	33.52	35.18	36.00	32.10	35.80
%C_{28}	31.78	24.38	31.35	31.58	29.27	29.70	34.40	30.60
%C_{29}	36.17	25.15	33.63	34.90	35.55	34.30	33.50	33.50
Diast/ster	0.43	0.05	0.22	0.23	0.28	0.31	0.44	0.35
%20S C_{29}	0.32	0.30	0.38	0.39	0.35	0.42	0.47	0.45
%ββR C_{29}	0.39	0.38	0.40	0.40	0.40	0.40	0.45	0.45
Phenanthrenes (*m/z* 178), dibenzothiophenes (*m/z* 184) and methylphenanthrene (*m/z* 192)								
DBT/P	0.11	0.27	0.39	0.27	0.34	0.51	0.51	0.61
MPI	0.77	0.96	0.61	0.68	0.58	0.78	0.73	0.80
%Rc	0.86	0.97	0.77	0.78	0.75	0.87	0.84	0.88

$\delta^{13}C_{Saturates}$= Stable carbon isotopic composition (‰) of the saturated HC fraction; $\delta^{13}C_{aromatics}$= Stable carbon isotopic composition (‰) of the aromatic HC fraction; Canonical variable (CV) = –2.53 $^{13}\delta C_{SAT}$ + 2.22 $\delta^{13}C_{ARO}$ – 11.65; C_{19}/C_{23} = C_{19}/C_{23} tricyclic terpanes; C_{22}/C_{21} = C_{22}/C_{21} tricyclic terpanes; C_{24}/C_{23} = C_{24}/C_{23} tricyclic terpanes; C_{25}/C_{26} = C_{25}/C_{26} tricyclic terpanes; Tet/C_{26} = C_{24} tetracyclic terpanes/C_{26} tricyclic terpanes; C_{29}/H = C_{29} norhopane/C_{30} hopane; OL/H = Oleanane/C_{30} hopane; G/C_{30}H = gammacerane/C_{30} hopane; $C_{35}S/H_{34}S$ = $C_{35}S/C_{34}S$ homohopanes; S/H =

steranes/hopanes; $\%C_{32}S$ = 22S/(22S+22R) C_{32} hopane ratio; $\%C_{27}$ (*m/z* 217) = $100\times C_{27}R/(C_{27}R+C_{28}R+C_{29}R)$; $\%C_{28}$ (*m/z* 217) = $100\times C_{28}R/(C_{27}R+C_{28}R+C_{29}R)$; $\%C_{29}$ (*m/z* 217) = $100\times C_{29}R/(C_{27}R+C_{28}R+C_{29}R)$; Diast/ster = 13β(H),17α(H) 20S C_{27} diasterane/5α(H),14α(H),17α(H) 20R C_{27} regular sterane ratio; %20S C_{29} = 20S/(20S+20R) sterane ratio; %ββR C_{29} = αββ/(αββ+ααα) sterane ratio; DBT/P = Dibenzothiophene (DBT)/Phenanthrene (P); Methylphenanthrene index (MPI-1) = 1.5(2-MP + 3-MP)/(P + 1-MP + 9-MP); Calculated vitrinite reflectance (%Rc) = 0.6×MPI-1+0.4 (Radke et al., 1984).

Highlights

- The Upper Cretaceous–Paleocene to Lower Eocene rocks contain Type-II/III and Type III kerogen
- The Miocene rocks yield mainly Type-III to Type-II/III with gas-generating potential
- Migrating oil may have affected source potential indications of the samples analyzed
- Three palynofacies associations have been recorded from the succession
- The maturity parameters consistently indicate immature to early mature stages